AN INVESTIGATION OF TEMPORAL VARIABILITY IN JET AVAILABLE POTENTIAL ENERGY

by

Lindsey E. Nytes

A thesis submitted in partial fulfillment of

the requirements for the degree of

Master of Science

(Atmospheric and Oceanic Sciences)

at the

UNIVERSITY OF WISCONSIN-MADISON

2017

ABSTRACT

Available Potential Energy (APE) accumulates in the Upper Troposphere-Lower Stratosphere (UTLS) of the tropics from the integrated outflow mass of tropical convection and storms. Due to inertial and radiative trapping, APE leaves the tropical UTLS primarily through periodic mass exchange with the extratropics. The resulting budget of tropical APE therefore serves as an indicator of both total tropical convective activity and total extratropical interaction with the tropical UTLS. As the subtropical jet typically bounds the tropical APE and the associated elevated tropical tropopause on its extratropical boundaries, the tropical APE in the UTLS is defined to be the difference of APE across the subtropical jet, thus deemed the Jet Available Potential Energy (JAPE).

In this study, the periodic behavior of globally integrated tropical JAPE in the UTLS is examined based on a four times daily ERA-I reanalysis over 38 years. The intent of this study is to determine the prevailing frequencies of fluctuations of JAPE over the tropical belt and within an isentropic layer representative of the UTLS. Results of this analysis indicate variability associated with the buildup and loss of JAPE with time. The results suggest that significant spectral variance is found on both diurnal and annual cycles, presumably associated with zonal variability and convective processes. Seasonal cycles are also found, which are thought to be associated with the seasonal variability of global convective processes. Evidence will be presented suggesting that the fluctuation of the intensity of the tropical JAPE surplus results in a similar fluctuation of tropical-extratropical mass exchange in the UTLS.

ACKNOWLEDGEMENTS

There are many people who deserve recognition for their support as I worked toward the completion of this degree.

First and foremost, I must thank my advisor, Professor Greg Tripoli, for first introducing me to this topic for my undergraduate research, and for encouraging me to continue my research into graduate school. His passion for atmospheric research nothing short of inspiring and his patience in explaining, and often re-explaining, the foundation and implications of this topic will not be forgotten.

I would also like to recognize the faculty and staff of the Department of Atmospheric and Oceanic Sciences, from whom I have learned so much in what feels like a very short amount of time. In particular, I thank Professors Jon Martin and Dan Vimont, who took the time to review my work in its final stages. Their comments, questions, and editorial suggestions undoubtedly led to the betterment of my paper. Additionally, I thank Pete Pokrandt, for obtaining and preformatting the data I use, and for assisting me in sorting out the various user-induced errors I encountered while working with the UW-NMS and Vis5D.

I must also acknowledge my undergraduate and graduate classmates, as well as my colleagues in the Tripoli research group. Their discussions, advice, and camaraderie have pushed me to continue to explore new horizons and try things without first passing judgment. I will forever value the friends I found within the AOS community.

Finally, I express my sincere gratitude to my parents, sister, non-AOS friends, and boyfriend, Brian, who have stood by my side since the very beginning. They have been present for every obstacle and every triumph, always cheering me on. Without their love and unwavering support of everything I strive to be, I would have never made it this far.

Table of Contents

LIST OF FIGURES

LIST OF ABBREVIATIONS

APE	**A**vailable **P**otential **E**nergy
CPT	**C**old **P**oint **T**ropopause
ECMWF	**E**uropean **C**entre for **M**idrange **W**eather **F**orecasting
ENSO	**E**l **N**iño **S**outhern **O**scillation
ERA-I	**E**CMWF **Rea**nalysis - **I**nterim
JAPE	**J**et **A**vailable **P**otential **E**nergy
LZNR	**L**evel of **Z**ero **N**et **R**adiation
MJO	**M**adden **J**ulian **O**scillation
NCAR	**N**ational **C**enter for **A**tmospheric **R**esearch
NCEP	**N**ational **C**enters for **E**nvironmental **P**rediction
PSD	**P**ower **S**pectral **D**ensity
RCE	**R**adiative **C**onvective **E**quilibrium
RWT	**R**ossby **W**ave **T**rain
STJ	**S**ub**t**ropical **J**et
UTLS	**U**pper **T**roposphere/**L**ower **S**tratosphere
UW-NMS	**U**niversity of **W**isconsin **N**onhydrostatic **M**odeling **S**ystem

1. Introduction

The concept of atmospheric energy has been studied for well over a century. Early studies of global energetics sought to determine the source of energy behind phenomena on scales both small (Margules 1903), and large (Lorenz 1955; Dutton and Johnson 1967). By adapting known concepts of potential, internal and kinetic energies, the idea of available potential energy (APE) was born. Continued research has come to show that by determining the rate of APE production, the amount of kinetic energy generated by the fluid movement of the atmosphere can be estimated. (Pauluis 2007). This study explores a variation on APE, appropriately called jet available potential energy, as it is bounded and conducted through the subtropical jets.

1.1 Available Potential Energy

The first reference to available potential energy (APE) is thought to have been in a twentieth-century journal article, "On the energy of storms," where it was first called "available kinetic energy" (Margules 1903). Margules additionally called the sum of potential energy and internal energy the "total potential energy." This quantity was later deemed "convenient," but it did not adequately address the energy available for conversion into kinetic energy, as only a very small portion of the total potential energy is actually available for conversion into kinetic energy in storms (Holton 2004). From this need, the concept of available kinetic energy was defined as "the maximum gain of kinetic energy [which] equals the maximum amount of total potential energy available for conversion into kinetic energy under any adiabatic redistribution of mass" (Lorenz 1955).

Lorenz (1955) critiqued the application of this definition, as the storms Margules studied did not contain the fixed mass within fixed regions that were required. Instead, Lorenz applied the idea to a much larger concept: the general circulation of the whole atmosphere. He renamed the quantity "available potential energy," which emphasized the portion of existing total potential energy.

Under Lorenz's definition, APE must be characterized by the following four traits:

1. The sum of APE and kinetic energy must be conserved under adiabatic flow;
2. APE is entirely derived from the distribution of mass;
3. APE must equal zero when stratification is both horizontal and statically stable; and
4. APE will be positive if the stratification is not both horizontal and statically stable.

To satisfy these requirements, the average APE per unit of area of the earth's surface is calculated as:

$$\bar{A} = (1+\varkappa)^{-1} c_p g^{-1} p_0^{-\varkappa}{}_0 \int_0^{\infty} \left(\overline{p^{1+\varkappa}} - \bar{p}^{1+\varkappa}\right) d\,\theta \tag{1.1}$$

where $\varkappa$ equals the ratio R/c_p, θ denotes potential temperature, and the bar over $p^{1+\varkappa}$ is representative of the average over an isentropic surface. In a simpler form, APE may be calculated as:

$$APE = \frac{\rho - \rho_{mix}}{\rho} gz \tag{1.2}$$

where the denotation of *"mix*" represents the mixed atmosphere. By this definition, APE is the difference between the total potential energy found in a given state and its new value after

adiabatic mass redistribution results in horizontal stratification (American Meteorological Society 2012).

In concluding his paper, Lorenz suggests a model for the maintenance of APE where net heating in low latitudes and net cooling in high latitudes results in the production of zonal APE, which is nearly all converted into eddy APE. Some of this may be dissipated by lessening the temperature gradient of the eddies, with the rest converted into eddy kinetic energy. Although some of this may be dissipated by friction, the remainder will be converted into zonal kinetic energy. All zonal kinetic energy will then eventually be dissipated by friction, or reconverted to zonal APE to recirculate once more.

1.2 Tropical Atmospheric Mass

One source of APE is found within storms over the tropics. Diabatic and thus latent heating by tropical cyclones and convective storms introduce large fluxes of high entropy air mass into the upper troposphere/lower stratosphere (UTLS) (Anthes and Johnson 1968). The injection of this mass vertically expands the isentropic layers in which outflow occurs, which has the effect of pushing isentropic layers above the outflow upward and those below the outflow downward (Folkins et al. 2000).

Above 10 km, the tropical atmosphere can be characterized by isentropic layers that have been pushed upwards, thus giving rise to the tropical tropopause layer. (Gettleman and M. de F. Forster 2002). While the upwards expansion of isentropic layers has the possibility of cooling the temperature of said layers due to changes in pressure, layers below 10 km tend to be pushed down and warmed.

Isentropic layers may also be inflated due to radiational heating of the mass contained in each layer. This occurs increasingly above the level of zero net radiation (LZNR), which is located around 1 km below the cold point tropopause at 16-17 km (Gettelman et al. 2004). The LZNR, which Gettelman calls the "level of zero clear sky radiational heating," is caused by the cancellation between shortwave absorption by ozone, resulting in heating, and convective cloud-top cooling. The LZNR corresponds to an isentropic height above 340 K and below 390 K. Interestingly, 356 K is also near or at the isentropic level intersecting the vertical center of the subtropical jet stream. The LZNR does not exist in the extratropics, as the extratropical atmosphere absorbs less shortwave radiation than the equator, thus continuously releasing energy to space (Dopplick 1972).

The upward expansion of the tropical UTLS is associated with elevated levels of potential energy, compared to that in the Earth's atmosphere as whole at those isentropic or equivalent isobaric levels. Some adiabatic cooling of the layer may also occur from the upward expansion, but this can be countered by radiative warming above the LZNR. The resulting positive anomaly of potential energy in the tropics could presumably be converted to kinetic energy of extratropical waves or other weather when this high potential energy air is brought together with low potential energy air at the same isentropic or isobaric level.

1.3 The Subtropical Jet and Energy Transport

Originally, as suggested by Palmén (1961), the STJ was thought to form as a result of westerly angular momentum along the tropical troposphere. However, APE has also been shown to be fundamental in the formation of the subtropical jets, as APE is released across

the entire jet stream as it is transported from the tropics to the extratropics (Krishnamurti 1961a).

Krishnamurti's winter studies of the northern subtropical jet stream found no large sub-diurnal variability in the STJ core speed or direction. However, slight latitudinal variations were found to occur on a diurnal scale, with February presenting as the steadiest month and December and January containing the largest variations.

Observations and computations of mass circulation over STJ axes show a Hadley-like thermally direct system. This can be seen in Fig. 1.1 (Krishnamurti's Fig. 8), which depicts a strong mass circulation cell that moves poleward with winter hemisphere. Initial calculations showed this circulation would have strength to balance radiational cooling of tropical troposphere, as well as release kinetic energy for export to higher latitudes. In addition to releasing large amounts of energy, these circulations also transport zonal angular momentum into higher latitudes (Krishnamurti 1961b). This suggests that the STJ may act as a link between tropical and polar zones, as it permits movement of mass, energy, and angular momentum from the tropics, poleward.

1.4 Jet Available Potential Energy

In a calculation similar to that of Lorenz's APE, jet available potential energy (Tripoli and Nytes 2017) is defined as:

$$JAPE = \frac{\rho - \rho_{std}}{\rho} gz \tag{1.3}$$

where ρ is the air density, z is the geopotential height, g is the acceleration of gravity and the subscript "*std*" refers to the value of density at the equivalent height in a standard extratropical atmospheric sounding.

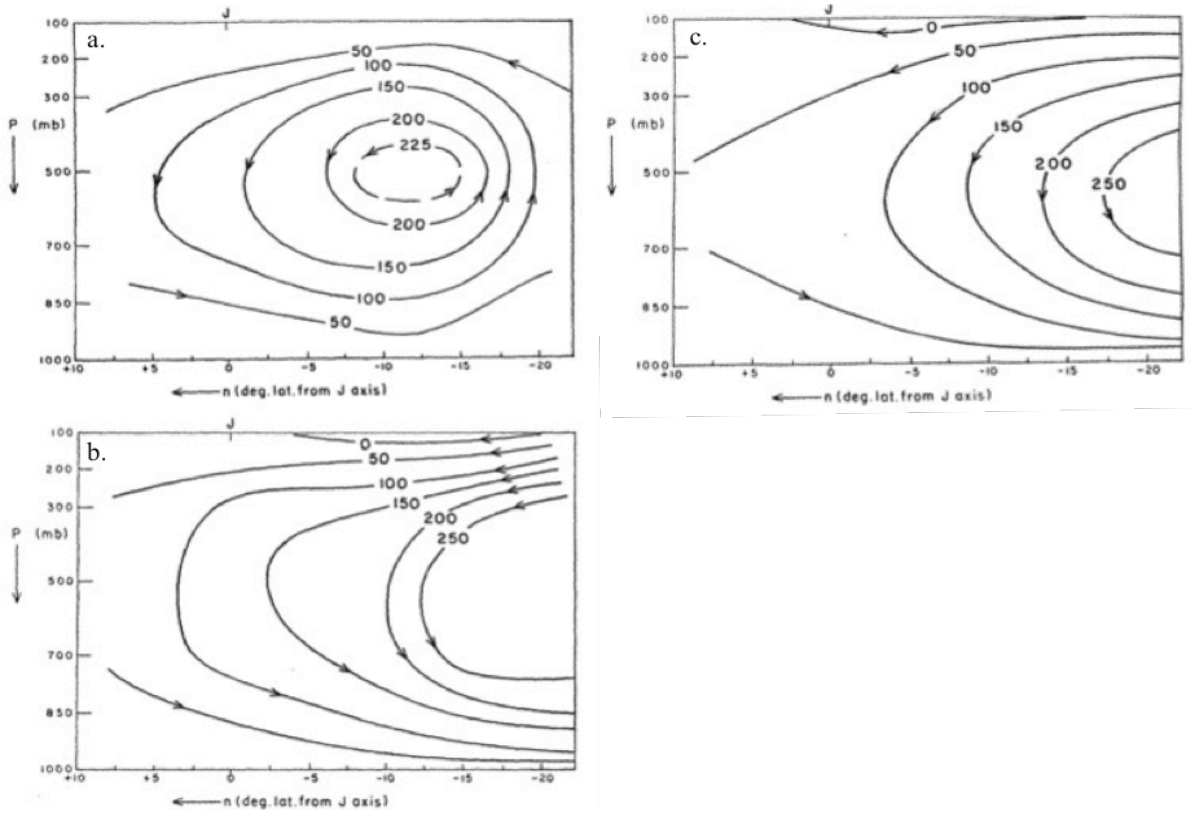

Figure 1.1: From Krisnamurti 1961, illustrating a strong mass circulation cell that moves poleward with the winter hemisphere. The mean cross section of the Stokes stream function is contoured in units of grams per sec. (a) December, (b) January, (February).

The standard sounding comes into use in order to address a commonly discussed drawback of Lorenz's APE. As mentioned by Pauluis (2007), APE is challenging to use as a diagnostic calculation of a real atmospheric potential for energy release, as the mixed state is never realistically approached, nor does it represent the locally relevant "relaxed" stated to which energy release responds. Instead, the tropical potential energy should be defined as available relative to the extratropical atmosphere to where the energy would be released. Since extratropical atmospheric states themselves are variable, a reasonable compromise is to compare the tropical potential energy to a mean or characteristic extratropical state, found in the "standard" extratropical sounding. By doing so, the relative energy in all tropical

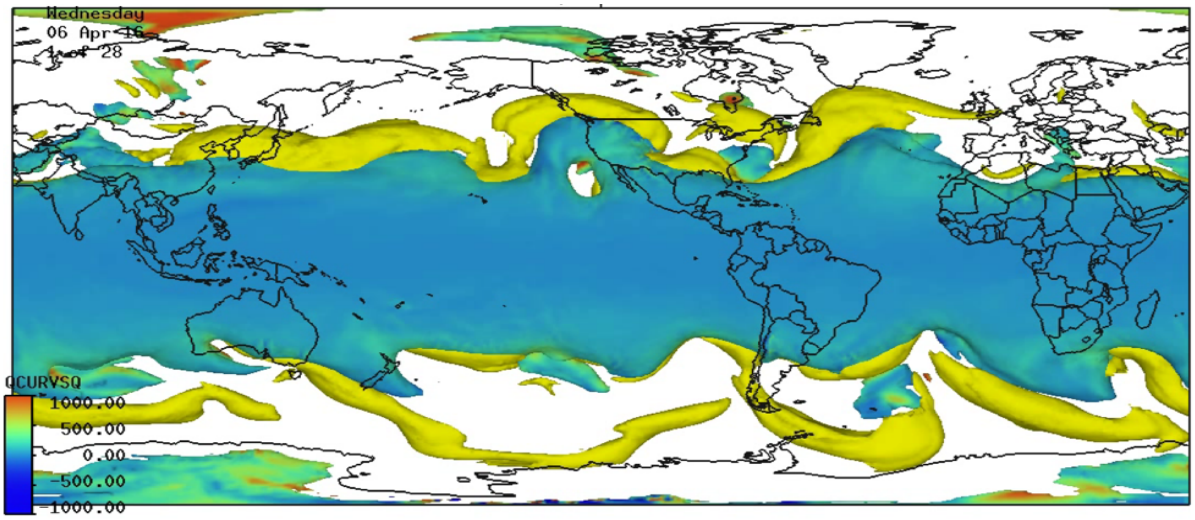

Figure 1.2: Top view of 2500 J/kg JAPE surface (colored by isentropic height) and jets (yellow surfaces) from NCEP/NCAR Reanalysis from 06 April 2016.

atmospheres can be compared to the same extratropical state and to each other.

By the definition given in Eq. 1.3, JAPE is the potential energy associated with the anomalous amount of mass suspended at a given altitude, relative to the standard sounding described above. As such, there tends to be a large JAPE "bubble" associated with the elevated tropopause in the tropics that is available if that upward expansion, relative to the mid latitudes, were to be relaxed. The JAPE bubble can be seen as a large surface over the tropics, bound by the subtropical jets, seen in Fig. 1.2. In such an interaction, JAPE energy could be converted to the kinetic energy of a subtropical jet stream, existing along the interface between the JAPE bubble and the extratropical atmosphere. As JAPE is the energy associated with the departure from a mean state, JAPE can maintain both positive and negative values.

In calculations of JAPE, isentropic coordinates replace the traditional isobaric coordinates. This substitution extends mass transport into the midlatitudes, as shown by Johnson (1989). In that paper, the use of isentropic coordinates leads to the discovery of a

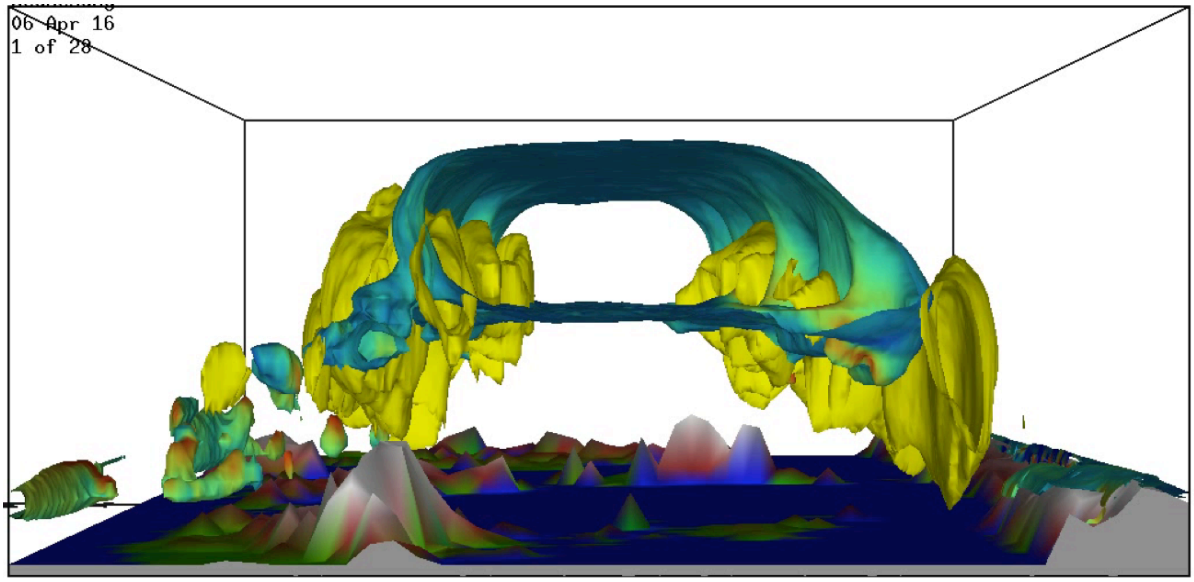

Figure 1.3: Eastward facing cross-section of the 2500 J/kg JAPE surface (blue green surface) and jets (yellow surfaces) on 12Z 06 April 2016, from NCEP/NCAR Reanalysis.

secondary part of the Hadley Cell, described as the geostrophic mode of mass transport. Positive JAPE values in the tropics tends to be confined between the 340K and 550K isentropic levels, with isentropic layers above 410 K pushed upward by work performed from heating below, but not significantly filled with diabatic fluxes of entropy.

Most of the JAPE bubble is above the upper extent of the tropical radiative convective equilibrium (RCE), bounded at the base by the LZNR and at the top by the CPT, found at 16-17 km or 380-390 K (Gettelman and M. de F. Forster 2002) Plotting the surface of the JAPE bubble, seen in Fig. 1.2, reveals that it is centered over the equator, with an average poleward boundary at latitudes around 30-35 degrees in either hemisphere. This can be attributed in part to the tropics containing the most angular momentum, being as far as possible from the Earth's axis of rotation.

The Earth's rotation creates inertial stability (Holton 2004), trapping energy aloft at the tropical tropopause and the subtropical jet. Although this was previewed in Fig. 1.2, it is

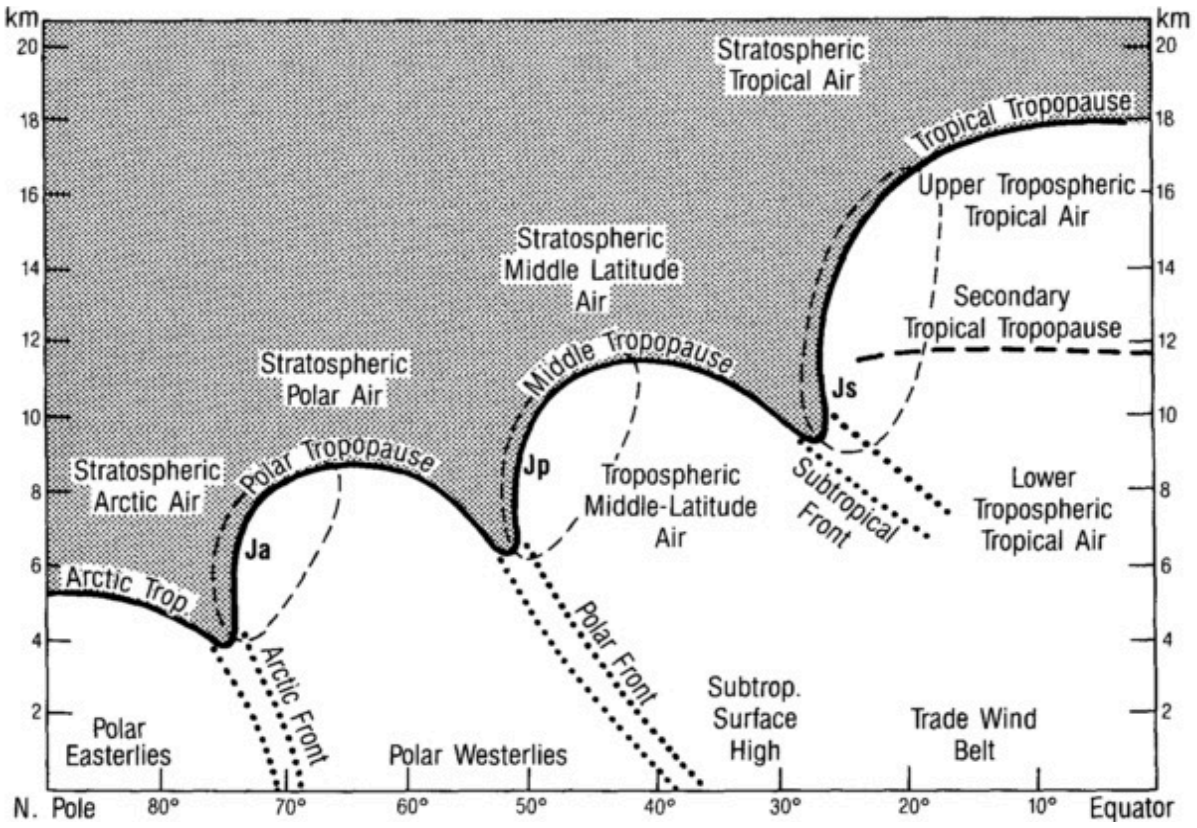

Figure 1.4: An idealized meridional model of the "threefold" structure of the tropopause. Relevant for this study are the tropopause from the potential vorticity discontinuity, indicated by heavy solid line; and 40 m s^{-1} isotachs representative of the arctic (Ja), polar (Jp), and subtropical (Js) jet cores, indicated by thin dashed lines (Shapiro et al. 1987).

easily seen in a cross section of the JAPE bubble (Fig. 1.3), where an eastward-facing visualization shows the bubble bounded on either side by the subtropical jets. An idealized meridional cross section (Fig. 1.4), illustrates the relative positions of the jets, with respect to the tropopause at different latitudes (Shapiro et al. 1987). Here, the subtropical jet is situated between 20˚N and 30˚N, with the tropical tropopause at a much higher altitude than the midlatitudinal tropopause. Likewise, the tropical tropopause is generally found at a high potential temperature (Chimonas and Rossi 1987).

The containment of JAPE by these boundaries can also be seen in Fig. 1.5, where

contours of isotachs greater than 32 ms^{-1} bound the JAPE bubble both north and south of the equator. Here, the tropopause is seen through the upward expansion of isentropes over the tropics, as well as the 1 PVU interval.

The total amount of JAPE stored within the tropical JAPE bubble is a quantitative measure of the cached tropical potential energy associated with the elevated tropical tropopause. It is not a pure measure of radiatively trapped energy as the isentropic layer elevation produced below and within the lower portion of the JAPE bubble can be altered from below adiabatically by the RCE process. However, significant layer compression below the JAPE bubble would be inconsistent with a state of true equilibrium and so is unlikely to occur.

Analysis of global reanalysis data shows that in the UTLS, JAPE, like APE, builds its energy content by the injection of high entropy by tropical convective systems and tropical cyclones into the lower and mid-UTLS. The amount of energy within the bubble, particularly in the upper portions above the LZNR, further increases diabatically from radiation absorption, growing upward toward the tropical CPT. In the lower troposphere, JAPE has a decreased tendency to build intensity over time since there is a net loss of energy by radiation to space, leading to RCE. Consequently, there is less of a tendency to build up a negative JAPE anomaly at low levels.

As the boundaries described above are finite, and JAPE is created continually from convection worldwide, some sort of mechanism must be in place to release energy from the bubble. Regular transfer of JAPE from the tropics poleward is thought to occur using the subtropical and polar jets as conduits. Plumes of JAPE are associated with powerful poleward eruptions mounded on the poleward side by a STJ, resulting in the transfer of JAPE

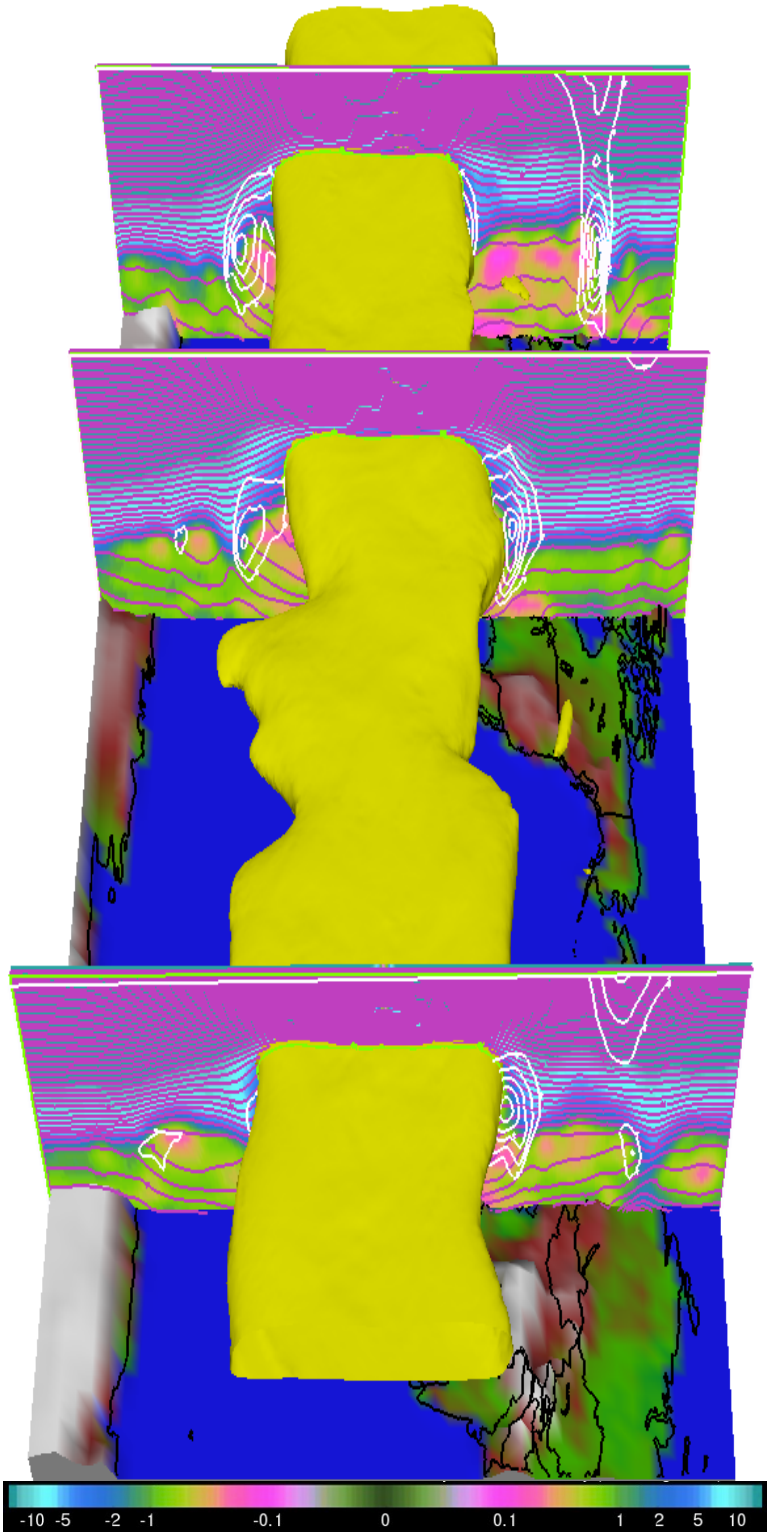

Figure 1.5: Westward facing cross-sections of 2500 J/kg JAPE, isotherms (contoured in pink every 10 K), westerly winds greater than 32 ms^{-1} (contoured in white every 10 ms^{-1}), and potential vorticity (PVU, log-scale seen below image) from NCEP/NCAR Reanalysis from 1200 Z 30 December 2016.

into the Rossby wave train (RWT). By energizing the upper part of the RWT circulation, the lower portion also is energized. Moreover, if the lower portion of the RWT already contains a polar jet, the energy of the JAPE bubble and its STJ could combine with or further enhance the polar jet. Alternatively, the STJ could spawn a lower level quasi-geostrophic circulation of its own, which would enhance any existing low-level thermal gradients, and therefore promote the growth of the STJ towards the surface.

When no interactions occur between the JAPE bubble and the subtropical jets, JAPE will continue to amass in its tropical reservoir. At some critical threshold, plumes of JAPE have been observed burst forth from the JAPE bubble, apparently due to weaknesses in the inertial resistance formed along the tropical tropopause fold, which are caused by the equatorward movement of anticyclonic vorticity on the equatorward side of the polar jet. These plumes begin as a poleward-arching region of the wall of the JAPE bubble, zonally spanning thousands of kilometers. The positive correlation of pressure forcing with velocity due to the poleward advance of the JAPE plume forces the conversion of JAPE to kinetic energy, thus accelerating the STJ along its poleward boundary. This takes the form of a poleward-arched STJ, where JAPE is actively converted to kinetic energy (Mecikalski and Tripoli 1998; 2003). Interestingly, this often appears to occur just poleward of an equatorward-arched polar jet, likely for reasons articulated above.

1.5 Thesis Motivation

It is evident from these studies and the 38-year analysis to be presented here, that the tropical and extratropical interactions supply an important contribution to the energy of the RWT and have a significant influence on extratropical weather. In this paper, the long-term

behavior of the potential energy stored in the tropical JAPE bubble will be examined based on reanalysis data over the last 38 years. The primary focus is on determining the periodicity of the build-up and release of JAPE, as well as making suggestions for the mechanisms behind such fluctuations.

Since the JAPE bubble has fluid boundaries and is not definitively contained at any given latitude, for this initial analysis the energy contained in the tropics and midlatitudes will be examined, an area which shall be defined for these purposes as the region of the planet with latitude at or less than 60 degrees. As such, the total integrated (mass weighted) JAPE bounded by two isentropic surfaces representing the UTLS and two latitude circles separating latitudinal zones will be monitored. Only positive values of JAPE will be included in the integrals to isolate the regions of tropical JAPE along the undulating poleward boundary of the JAPE bubble.

An outline of the remainder of this paper is as follows. Section 2 will describe the data, calculations, and statistical methods to be used leading to suggestions regarding the contributing vertical sources and sinks of JAPE over time. Sections 3 and 4 will contain time series and spectral analyses of the integrated JAPE and related layer mass calculated over the 38 years between 1979 and 2016. In Section 5, the average annual period will be analyzed to lend additional support to the hypotheses drawn. Finally, in Section 6, there will be a discussion of the implications of these results and conclusions will be made regarding the applications of JAPE, along with suggestions for the direction of future research.

2. Data & Methodology

This study will focus on the positive JAPE anomalies associated with the elevated tropical tropopause, from European Centre for Midrange Weather Forecasting (ECMWF) Reanalysis Interim (ERA-I) six-hourly data spanning the thirty-eight-year period from 00Z 01 January 1979 through 18Z 31 December 2016 (Dee et al. 2011). Additional data, from 00Z to 06Z on 01 January 2017 was obtained from the National Centers for Environmental Prediction/National Center for Atmospheric Research Reanalysis dataset (Kalnay et al. 1996) for the purpose of completing analysis of 2016. To simplify analysis, leap days have been removed from the data set. The spatial resolution of the data is approximately 1˚ by 1˚.

All data has been calculated from the ERA-I and NCEP/NCAR Reanalysis datasets using analysis tools in the University of Wisconsin Nonhydrostatic Modeling System (UW-NMS) (Tripoli and Smith 2014a,b). Data processing in the UW-NMS includes calculations of variables of interest and formatting for data analysis. The analysis calculates the long-term evolution of the integrated amount of potential energy stored in the elevated JAPE bubble. The integral, performed on a latitude-longitude or spherical grid, becomes:

$$[JAPE] = R_e^2 \int_{\varphi_1}^{\varphi_2} \int_{\lambda_1}^{\lambda_2} \int_{\theta_1}^{\theta_2} JAPE\ \rho \frac{dz}{d\theta} d\theta\ cos\varphi\ d\lambda\ d\varphi \tag{2.1}$$

where $[JAPE]$ is the mass integral of JAPE, R_e is the radius of the Earth, φ is the latitude angle in radians, and λ is the longitude angle in radians.

The JAPE bubble is suspended over isentropic layers, which are inflated either with mass injected diabatically by convective plumes, or by radiation, particularly above the layer of zero net radiation. This injected mass is representative of the entropy associated with the potential temperature of the layer where it is inserted. The mass is considered radiatively

trapped since it may only breach the layer it occupies through diabatic processes. Therefore, monitoring the variability of this layer mass can be considered an additional diagnostic of the build-up of trapped entropy in the JAPE bubble. Similar to the isentropic JAPE, total isentropic layer mass is computed as:

$$[M] = R_e^2 \int_{\varphi_1}^{\varphi_2} \int_{\lambda_1}^{\lambda_2} \int_{\theta_1}^{\theta_2} \rho \frac{dz}{d\theta} d\theta \, cos\varphi \, d\lambda \, d\varphi \tag{2.2}$$

where $[M]$ is the integral isentropic mass, φ is the latitude angle in radians, λ is the longitude angle in radians and θ is the potential temperature in K. This results in a measurement of the total mass contained between isentropic layers (θ_1, θ_2) of the JAPE bubble. The total storage within prescribed isentropic layers will be confined to the tropical troposphere above the level of zero net radiation at 356K and below 420 K, a layer representative of the UTLS.

For these measurements, the range of longitude, λ, will consist of the entire zonal region of the globe. Four separate latitudinal regions will comprise the φ component: 30˚N-60˚N ("north midlatitudes), 60˚S-30˚S ("south midlatitudes"), 30˚S-30˚N ("tropics"), and 60˚S-60˚N ("nonpolar region"). By using latitudinal regions, the data is essentially averaged over each prescribed area on the global scale.

The midlatitudes of both hemispheres are important to consider due to the extratropical interactions with the JAPE bubble that allow energy to breach the inertial wall. The tropics host the core of the bubble, as well as some of the plumes of energy leaving the bubble. Finally, the nonpolar region, encompassing both tropics and midlatitudes, allows for comparison of said regions as it effectively closes the system. For the sake of equal comparison, these latitudinal regions will be used in analysis of all quantities considered.

After using time series analysis to gain an overview of the occurring periods and associated amplitudes, spectral analysis will be performed to further isolate and assess the significance of the frequencies of energy fluctuations in the JAPE bubble. This is accomplished by computing the power spectral density (PSD) through the use of Welch's overlapped segment averaging estimator, which essentially averages modified periodograms by multiplying segments of the time series by a window function (MathWorks 2017). For this analysis, a Hamming window function is used, with 50 percent overlap between windows.

Statistical significance is computed via chi-squared testing with 99.99% confidence limits. The Chi-Squared Statistic is defined in Hartmann (2005) as:

$$\chi^2 = \frac{(N-1)s^2}{\sigma^2} \tag{2.2}$$

The null hypothesis for computing statistical significance is an AR(2) process computed from the entire time series.

In Section 4, average annual periods are calculated by first averaging together each day's four data points into one daily value. Then, each calendar date is averaged across the entire 38-year data set, to arrive at a final product of an "average year." This is performed for each of the four latitudinal regions for both isentropic JAPE and layer mass, for the 356-420 K layer.

As this is a large, multi-decade set of data, it should be possible to see fluctuations in levels of JAPE at consistent frequencies based on regularly occurring atmospheric patterns such as the diurnal cycle, Madden-Julian Oscillations (MJO), and the annual cycle. Multi-year oscillations, such as the El Niño Southern Oscillation (ENSO), Pacific Decadal Oscillation (PDO), Atlantic Multidecadal Oscillation (AMO), and the sun cycle should also

be apparent. However, taking into consideration that this study will focus on only thirty-eight years of data, the primary peaks in power are predicted to occur on diurnal through annual frequencies.

3. Time Series Analysis

The fluctuations in the amount of isentropic JAPE and layer mass over the course of 38 years in the 356-420 K isentropic layer can be seen in Figs. 3.1-3.4. Across all latitudinal regions, the regular rise and fall of the values of JAPE is clear. However, the differences and similarities between regions are equally apparent, and considerably more interesting.

3.1 JAPE

Figs. 3.1a and 3.1b depict the integrated JAPE found in the north and south midlatitudes, defined earlier as 30˚N-60˚N and 30˚S-60˚S, respectively. The time series for these two regions reflect a near-identical pattern of periodicity, which is offset by roughly half of a year. The magnitude of the JAPE bubble shows to be the primary difference between the two hemispheres. These regions at first glance are rather unremarkable, with an apparent annual cycle of roughly equal amplitude year-to-year, lacking support of large-scale variability on the 38-year time range. On a smaller scale, periods of seasonal and short-term variability are hinted at, but are effectively lost within the annual cycle. Patterns of variability greater than one year are not seen in either of the two series. The lag between the north and the south midlatitudes is confirmed through comparison of Figs. 3.1b and 3.1d, where the maximum of one period occurs during the minimum of the other. By isolating a single year in both regions, it is easier to see shorter periods of energy fluctuation, although patterns are not easily recognizable.

Patterns of variability become much more complex upon looking at Figs. 3.2a and 3.2b, which represent integrated JAPE in the tropics and the nonpolar region, defined earlier as 30˚S-30˚N and 60˚S-60˚N, respectively. As seen before with the midlatitudinal time

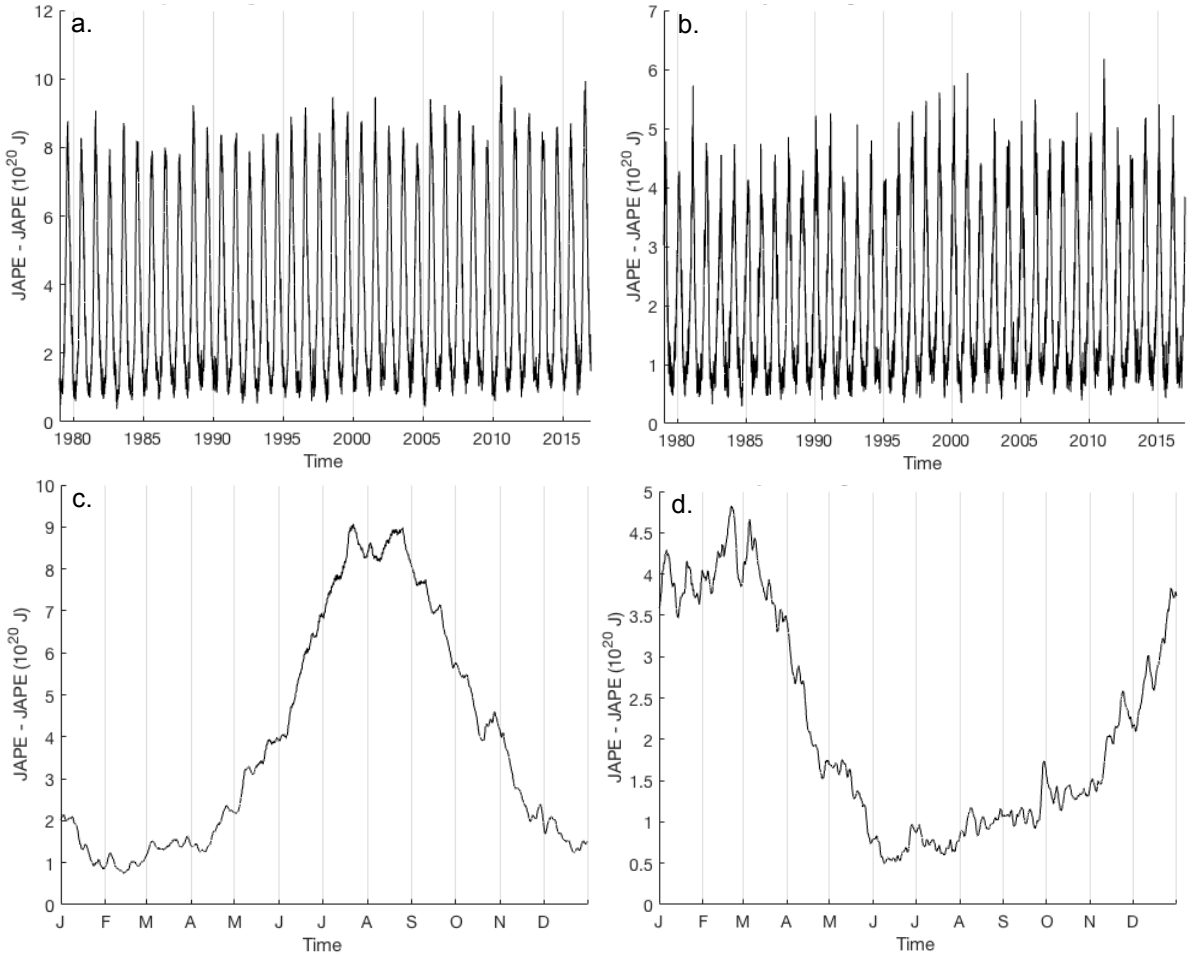

Figure 3.1: Time series of JAPE in the 356 K-420 K isentropic layer. (a) North midlatitudes (30˚N-60˚N) over the 38-year period from 00Z 01 January 1979 to 18Z 31 December 2016. (b) South midlatitudes (30˚S-60˚S) over the 38-year period from 00Z 01 January 1979 to 18Z 31 December 2016. (c) North midlatitudes over the 1-year period from 00Z 01 January 2007 to 18Z 31 December 2007. (d) South midlatitudes over the 1-year period from 00Z 01 January 2007 to 18Z 31 December 2007.

series', these time series look similar to each other at first glance. Additionally, an annual cycle is still apparent, although it is not found to quite the same extent as seen in the midlatitudes, as there is increased variability in the amplitude of the annual cycle. Large-scale variability is missing as well from these regions; however, seasonal variability is much more apparent in these regions.

The differences and similarities between the four regions help in forming hypotheses

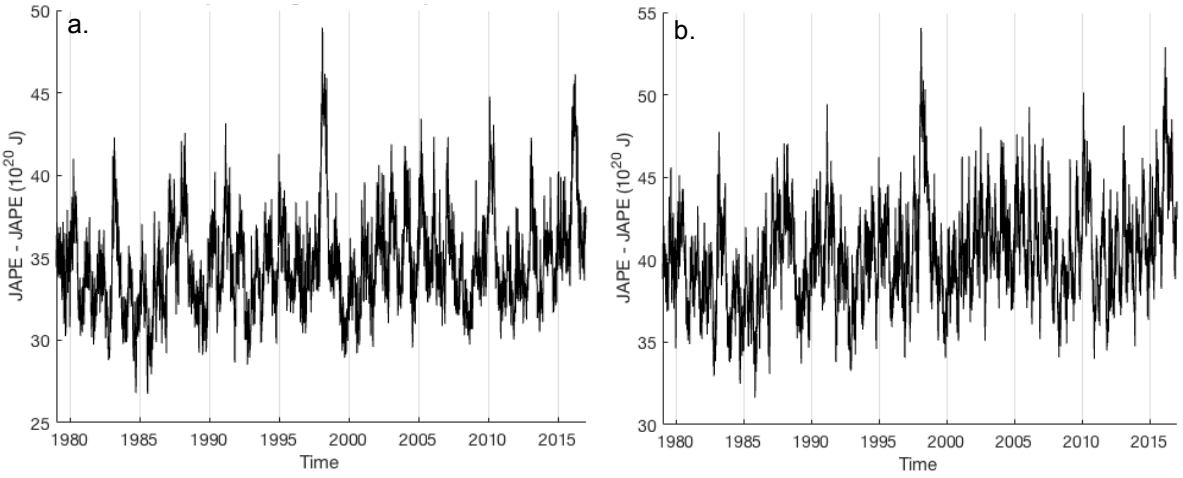

Figure 3.2: Time series of isentropic JAPE in the 356 K-420 K layer over the 38-year period from 00Z 01 January 1979 to 18Z 31 December 2016. (a) Tropics (30˚S-30˚N). (b) Non-polar region (60˚S-60˚N).

on the spatial range of the JAPE bubble. As seen in comparison of Figs. 3.1a and 3.1c to Figs. 3.1b and 3.1d, the north midlatitudes typically report a higher value of JAPE. This suggests two possible hypotheses: the JAPE bubble may be centered slightly north of the equator, or the bubble may have more frequent or stronger plumes to transfer JAPE out of the tropics.

In comparing the magnitude of JAPE found in either of the midlatitudinal regions to that found in the tropics, it is found that the tropics host the bulk of the JAPE bubble. As seen earlier in spatial plots in Figs. 1.1 and 1.2, this is not unexpected. Similarly, the similarities seen between the tropical and nonpolar time series' are also to be expected. As the nonpolar region encompasses the tropics and the midlatitudes in either hemisphere, and the average value of JAPE in the tropics is 4 to 10 times that of the midlatitudes, it follows that the nonpolar time series closely mimics that of the tropics. The difference in amount of JAPE present in each region can be inferred from Fig 3.3, which plots the four 38-year time series of JAPE on one figure.

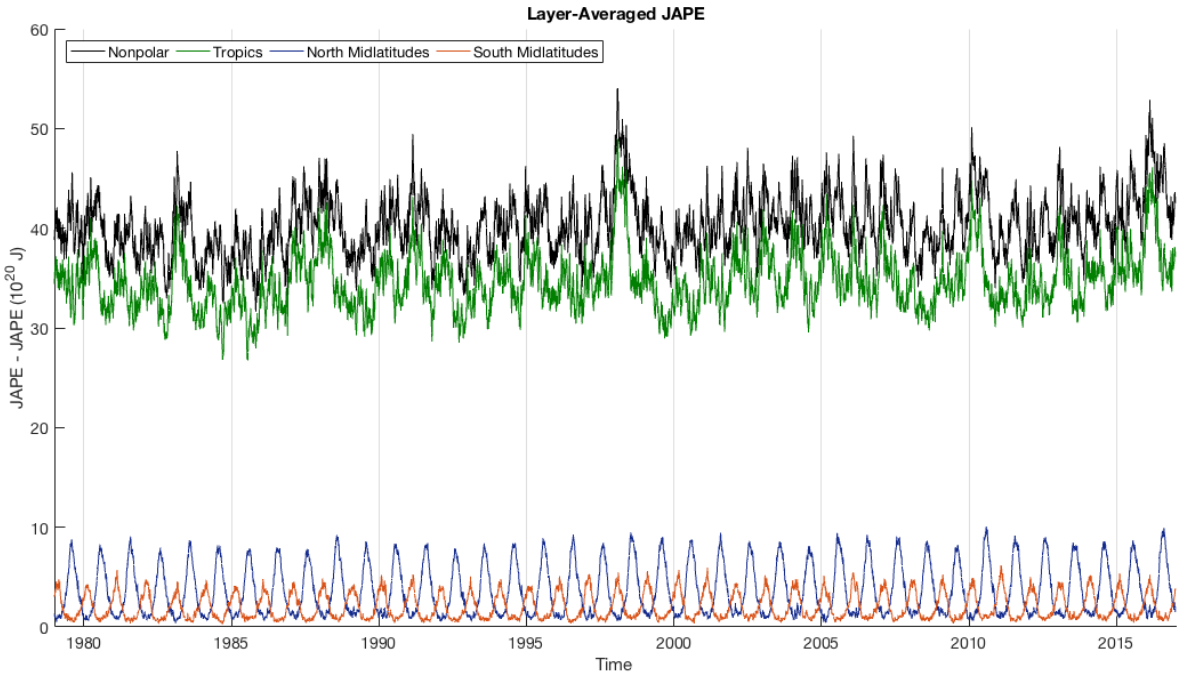

Figure 3.3: Combined time series of isentropic JAPE in the 356 K-420 K layer over the 38-year period from 00Z 01 January 1979 to 18Z 31 December 2016, showing the north midlatitudes (blue), south midlatitudes (red), tropics (green) and nonpolar regions (black).

A Hovmöller diagram of a single year at 364 K (Fig. 3.4) displays fluctuations of the JAPE bubble, showing its latitudinal dependence. Here, the annual cycle is still the most easily seen, as the bubble shifts from one hemisphere to the other. Inside the bubble, JAPE appears to increase and decrease with some degree of regularity, additionally supporting the suggestion of short-term variability in the tropics.

3.2 Layer Mass

Due to inherent similarities between isentropic JAPE and layer mass, one could hypothesize that a time series of layer mass would look much like one of JAPE. This quantity is based on the same mass used in the integration of JAPE, but instead not weighted by the value of JAPE. Also, regions of negative JAPE are not excluded from the integration as they are for the calculation of JAPE, perhaps leading to greater differences of the calculation in

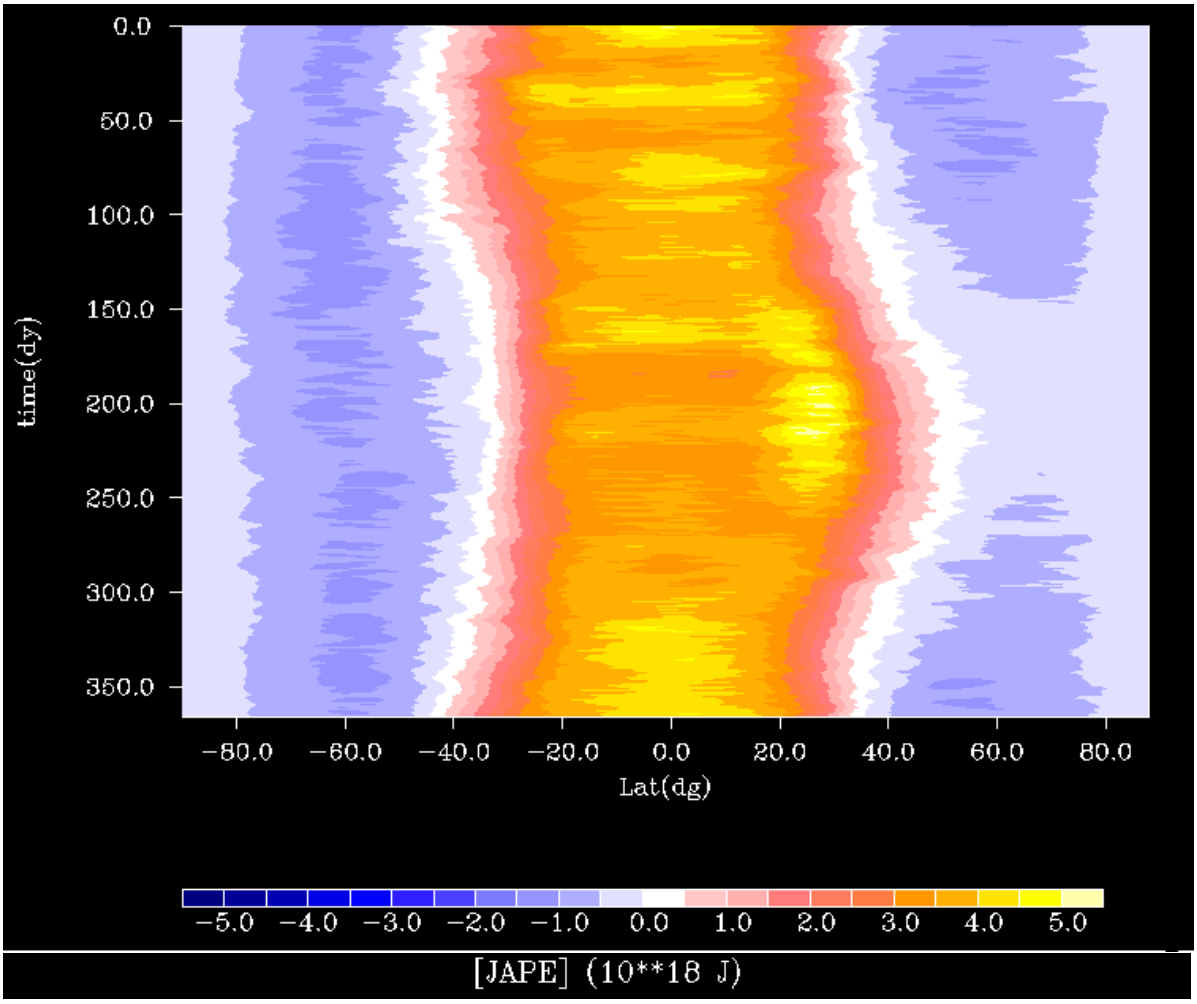

Figure 3.4: Hovmöller diagram of the JAPE bubble as it varies with time (vertical axis) and latitude (horizontal axis), found at a height of 364 K. Units of time are in days from 01 January 2013.

the middle latitudes where the poleward boundary of positive JAPE is most often found. Fig. 3.5 depicts the isentropic mass found in the north and south midlatitudes, tropics, and nonpolar region, as it fluctuates over the course of the 38-year period.

Comparing the layer mass to JAPE in the two midlatitudes (Figs. 3.5a and 3.5b) shows more varied time series – the amplitude of the annual period in both hemispheres is considerably less constant from year to year, and short-term variability is more apparent than before. The difference in magnitude of mass between the north and south midlatitudes is also

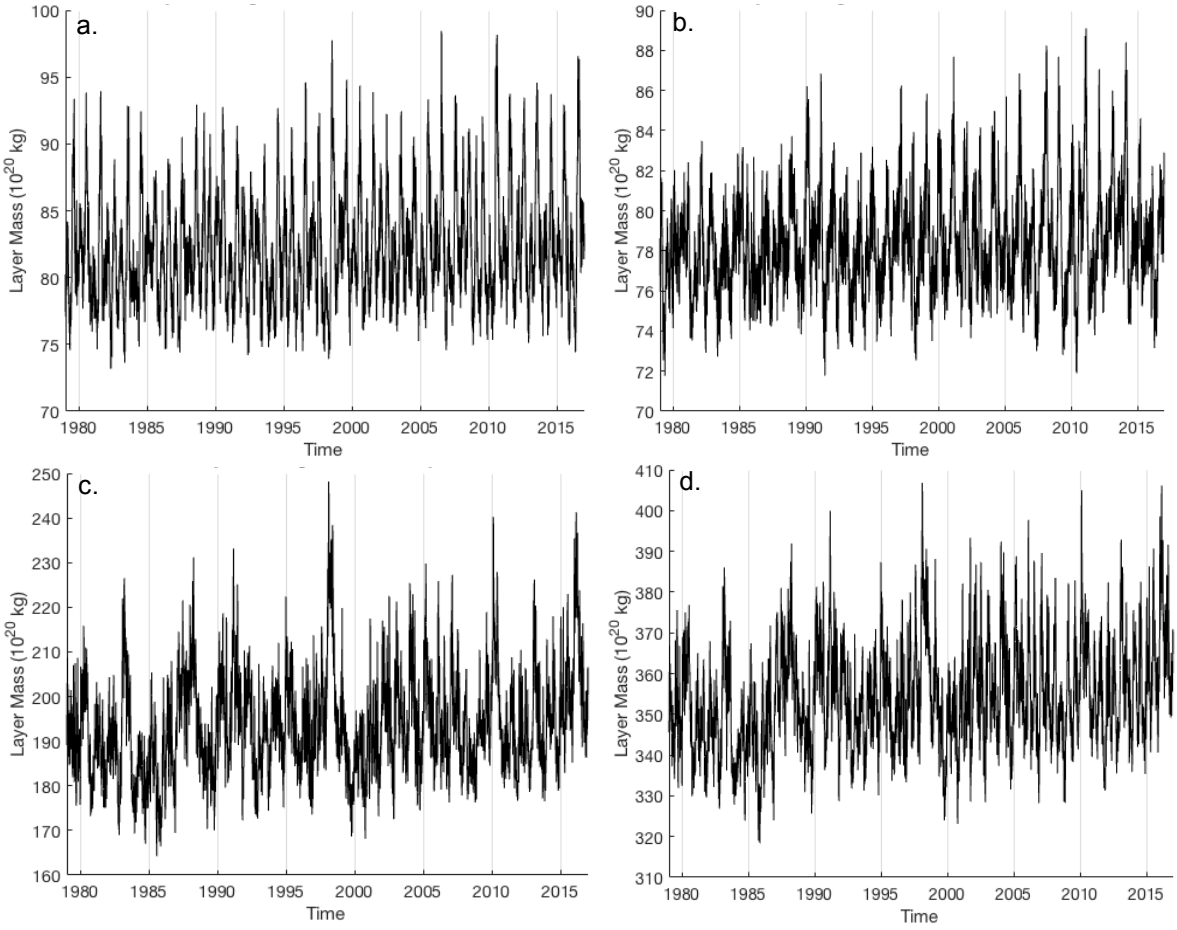

Figure 3.5: Time series of isentropic mass in the 356 K-420 K layer over the 38-year period from 00Z 01 January 1979 to 18Z 31 December 2016. (a) North midlatitudes (30˚N-60˚N). (b) South midlatitudes (30˚S-60˚S). (c) Tropics (30˚S-30˚N). (d) Non-polar regions (60˚S-60˚N).

much smaller. This can also be said of the difference in magnitude between either of the midlatitudinal regions and the tropics, seen in Fig 3.5c.

The time series for tropical layer mass looks highly similar to the time series for tropical JAPE, seen in Figs. 3.2a. An annual cycle is still present, with some short-term variability as well. Finally, the nonpolar layer mass (Fig. 3.5d) retains some similarity to its JAPE companion. The same maxima are still present, although the gaps between the peaks are filled in. The differences in magnitude between tropical and nonpolar layer mass is

considerably higher than found earlier in JAPE, which can be attributed to the decreased difference in magnitude between tropical and midlatitudinal layer mass. This would suggest that the midlatitudes might have a greater influence on the patterns of nonpolar layer mass than they had on the patterns of nonpolar JAPE.

4. Spectral Analysis

Time series analysis of isentropic JAPE and layer mass shows patterns of periodicity occurring in all regions analyzed. In order to gain further insight about the significance of these periods, performing spectral analysis by computing the PSD of JAPE and layer mass results in the confirmation of several significant periods in each region.

4.1 JAPE

The spectrum of isentropic JAPE observed in the north midlatitudes (Fig. 4.1a) contains significant periods of 182.8 and 366.0 days per cycle. These values are averaged, as significant periods at 173.4, 182.5, and 192.6, as well as 346.7 and 385.3, are part of the same distinct peak. The coordinating spectrum of JAPE in the south midlatitudes (Fig. 4.1b) appears to be similar to that of the north midlatitudes. Significant periods of 182.8 and 366.0 (on average) days per cycle are clearly seen. In both spectra, peaks are also seen at 0.5, 1, and 121.7 days per cycle. However, in neither spectrum do these values surpass the confidence levels required to achieve statistical significance.

Spectral analysis of the tropics yields a different set of significant periods to consider, seen in Fig. 4.1c. Significant periods are seen prominently at 0.5, 1.0, and 366.0 days per cycle, on average. Finally, this layer as found over the nonpolar region yields peaks nearly identical to those seen over the tropics, with significant periods found at 0.5, 1.0, 366.0, on average (Fig. 4.1d). Although it was lacking from the tropical spectrum, the 182.8-day period seen earlier in the midlatitudes is present again with the nonpolar spectrum.

As suggested with time series analysis, the north and the south midlatitudes share highly similar periodicity. Both regions exhibit an annual and a semiannual cycle, both of

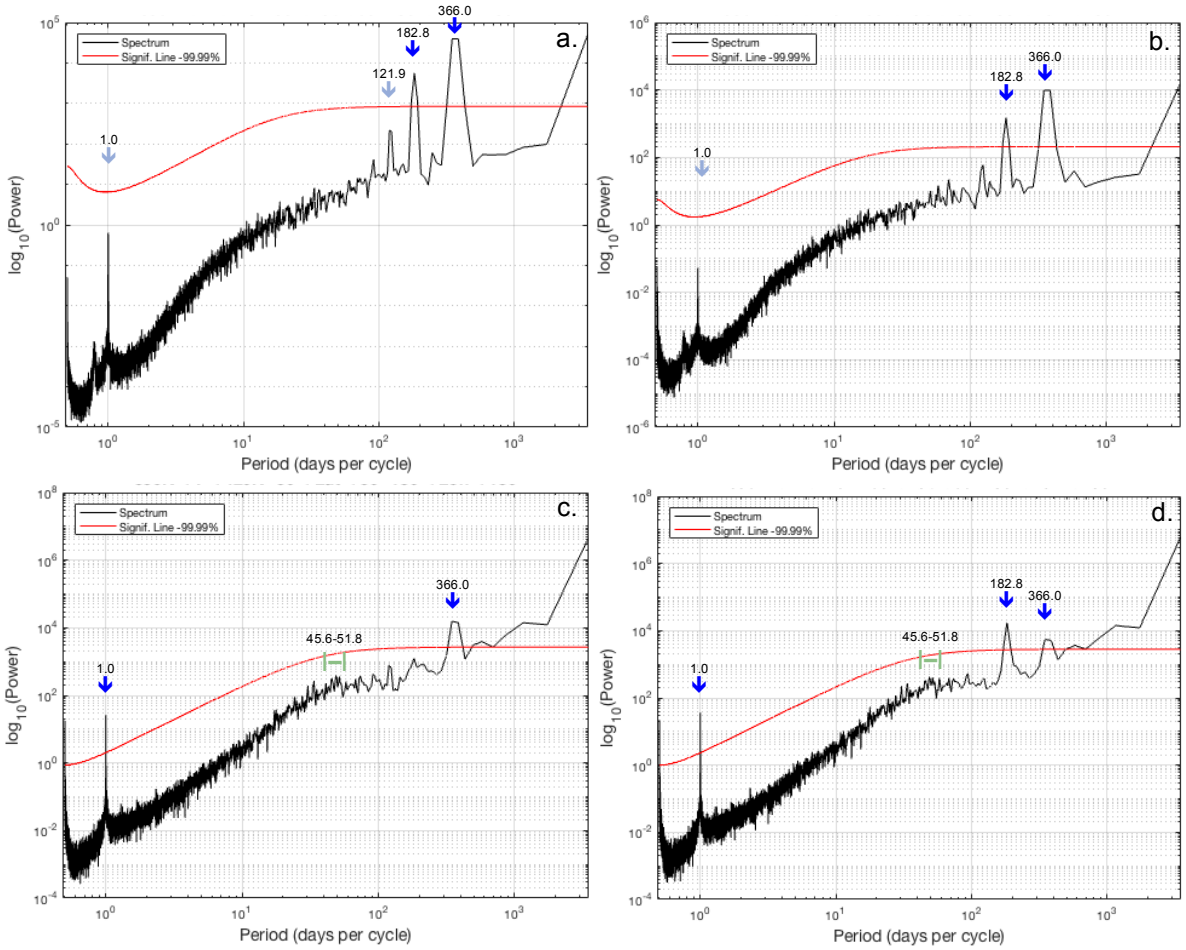

Figure 4.1: Spectral analysis of isentropic JAPE at the 356 K-420 K layer over the 38-year period. The solid red line represents statistical significance at 99.99% confidence levels. Bright blue arrows indicate periods that are statistically significant, light blue arrows indicate periods that are prominent but not statistically significant. Additional interesting features indicated by green brackets. (a) North midlatitudes (30˚N-60˚N). (b) South midlatitudes (30˚S-60˚S). (c) Tropics (30˚S-30˚N). (d) Non-polar regions (60˚S-60˚N).

which are significant at 99.99%. Additionally, a signal is seen for diurnal and semidiurnal cycles, although in neither region are they statistically significant. Finally, the north midlatitudinal time series also displays a prominent yet not significant spectral peak at 121.9 days, which is not seen at nearly the same magnitude in the south midlatitudes.

Spectral analysis in both the tropics and nonpolar region reveals statistically significant annual, diurnal, and semidiurnal cycles. The seasonal cycle seen before in the

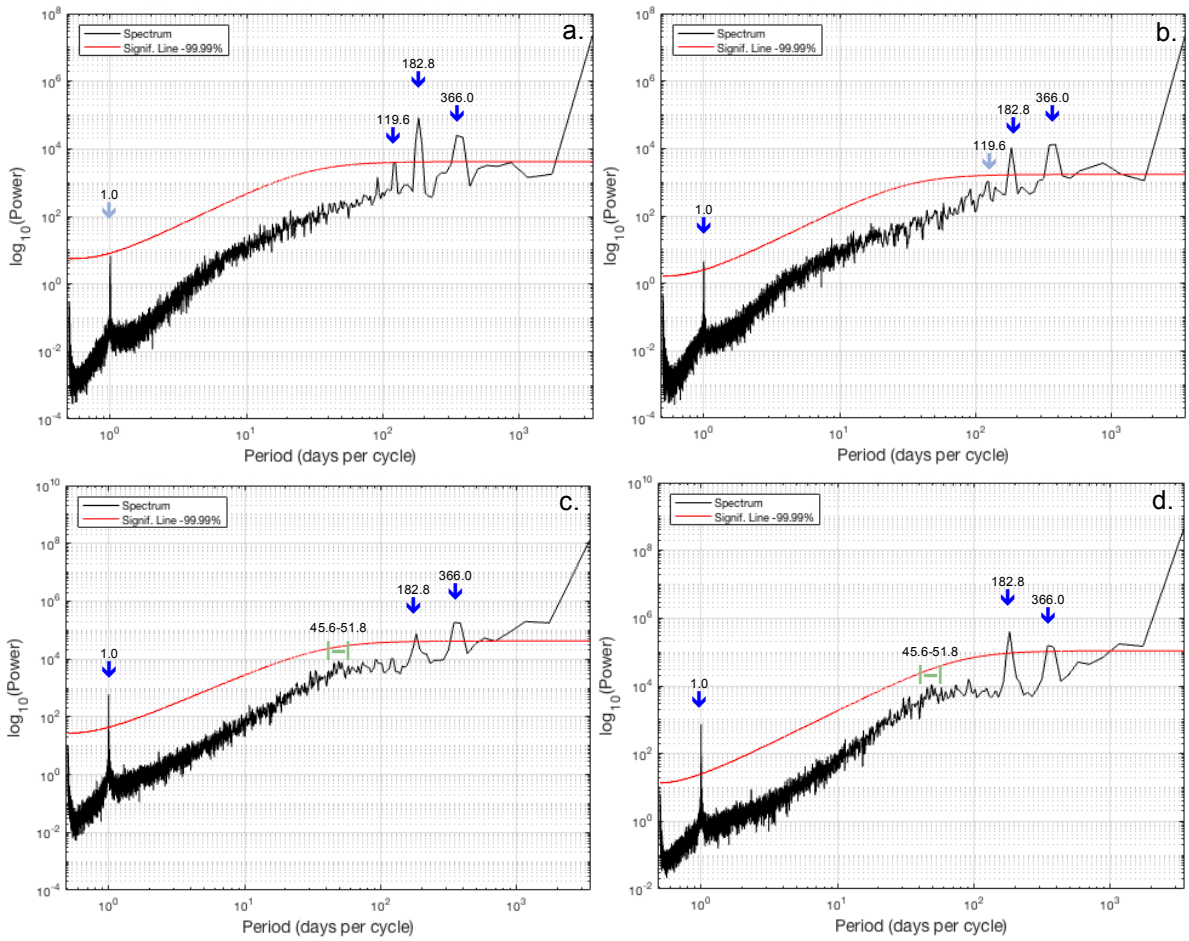

Figure 4.2: Spectral analysis of isentropic mass at the 356 K-420 K layer over the 38-year period. The solid red line represents statistical significance at 99.99% confidence levels. Bright blue arrows indicate periods that are statistically significant, light blue arrows indicate periods that are prominent but not statistically significant. Additional interesting features indicated by green brackets. (a) North midlatitudes (30˚N-60˚N). (b) South midlatitudes (30˚S-60˚S). (c) Tropics (30˚S-30˚N). (d) Non-polar regions (60˚S-60˚N).

midlatitudes is not significantly present in the tropics; however, it is seen once again, unsurprisingly in the nonpolar region. There is an isolated cluster of frequencies seen in both tropical and nonpolar spectra, with periods ranging from 45.6 to 51.8 days. This cluster does not achieve statistical significance here, but remains of interest due to potential connections to tropical-extratropical interactions.

4.2 Layer Mass

Spectral analysis of isentropic layer mass confirms the similarities and differences discovered with time series analysis in Section 3. In the north midlatitudes (Fig. 4.2a), significant periods are found at 119.6, 182.8, and 366.0 days per cycle. Prominent periods are also seen at 0.5, 1.0, and 91.25 days, although they do not achieve statistical significance. The south midlatitudes (Fig. 4.2b) trades the significance of the 119.6-day period for the 1.0-day period, in addition to retaining the significant annual and semiannual periods. In fact, the 119.6- and 91.25-day periods are not nearly so prominent as they were in the north midlatitudes.

This pattern is repeated for the spectra of tropical and nonpolar isentropic mass, seen in Figs. 4.2c and 4.2d. Significant cycles are found at 1.0, 182.5, and 366.0 days, while the 0.5-day period remains prominent, yet not statistically significant. The cluster of frequencies from the spectra of JAPE is present once more with layer mass, where periods range from 45.6 to 51.8 days. This cluster still does not achieve statistical significance for this quantity, but will merit additional investigation due to potential implications.

5. Average Annual Period

Averages of the annual period of the entire 38-year set of JAPE and layer mass data remove the semidiurnal and diurnal cycles to isolate larger scale variability and create the time series for an "average" year for the 356-420 K layer in all regions previously discussed.

5.1 JAPE

In the north midlatitudes (Fig. 5.1a), the maximum in JAPE is seen at the start of August, while the minimum is seen towards the end of February. Overall, the average annual period is very smooth, showing very little for short-term variability. Most notable in this figure is the high contrast seen between the maximum and minimum – the quantity of JAPE at the maximum is approximately 8 times that at the minimum.

The south midlatitudes (Fig. 5.1b) have a similar, opposing pattern to that seen in the north midlatitudes. Here, the maximum in JAPE is found at the start of February, while the minimum is found in a low plateau over the months of July and August. Also like the north midlatitudes, the south midlatitudes contain a smooth average annual period with little for short-term variability. However, here a much lower contrast is seen between the maximum and minimum values, with only half the amplitude seen in the northern counterpart.

The average annual period for the tropics (Fig. 5.1c) shows a pattern differing from those seen in the midlatitudes. Like the south midlatitudes, a maximum in JAPE is seen in early February, with a minimum found in September. In addition to these absolute values, relative maxima/minima pairs are seen every one to two months. In comparison to the midlatitudes, this jagged average annual period suggests that the tropics may contain more short-term variability. It is also worth noting that the magnitude of JAPE found at the tropics

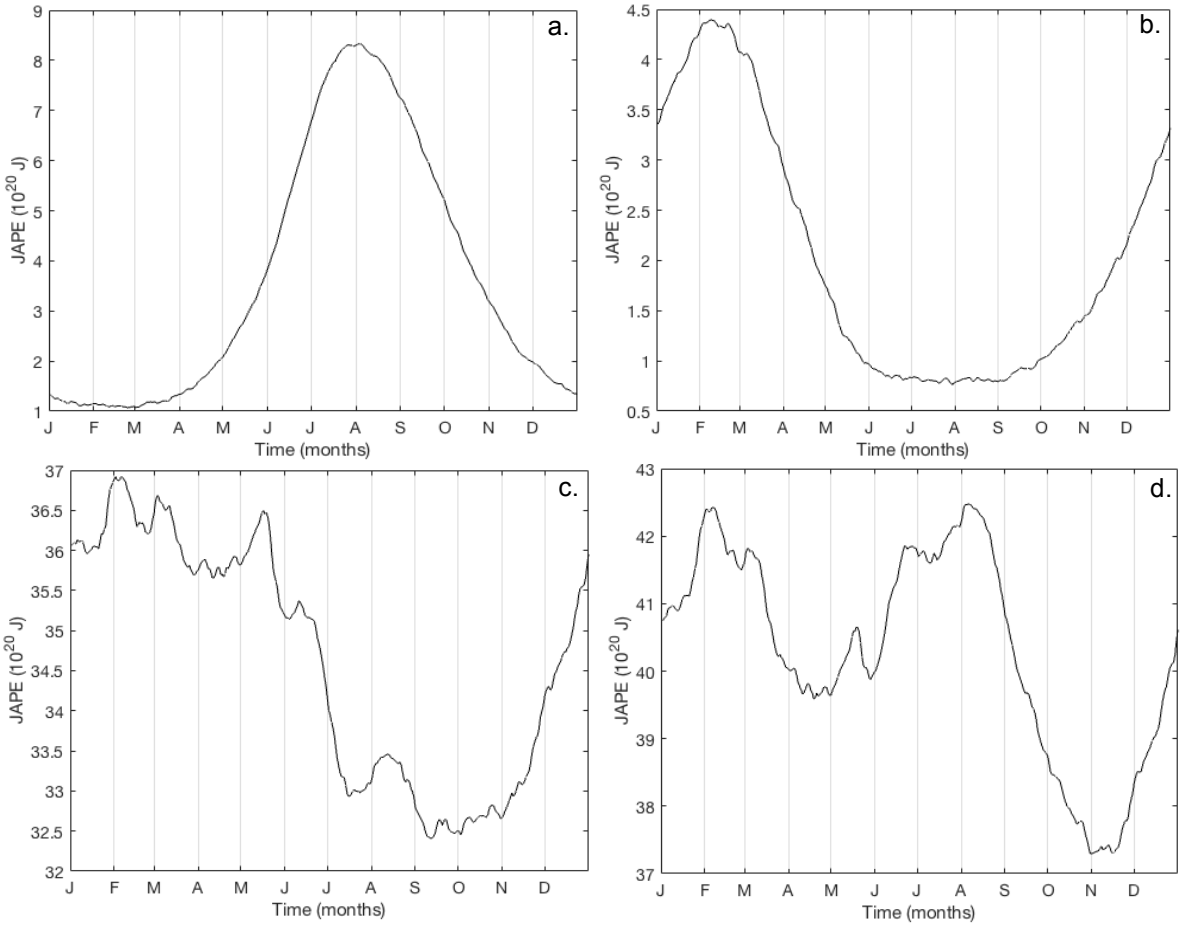

Figure 5.1: Average annual period of isentropic JAPE at the 356 K-420 K layer, calculated from the entire the 38-year period. (a) North midlatitudes (30˚N-60˚N). (b) South midlatitudes (30˚S-60˚S). (c) Tropics (30˚S-30˚N). (d) Non-polar regions (60˚S-60˚N).

is still larger in the average annual year than that seen in the midlatitudes combined.

Finally, the average annual period of the nonpolar region (Fig. 5.1d) has an appearance most similar to that of the tropics, including the maximum found in early February, and increased short-term variability compared to the midlatitudes. However, a secondary maximum is found in early August, with amplitude nearly equal to the earlier maximum. Additionally, the minimum of the period is pushed back to November. Although less jagged than the tropics, the nonpolar region still contains more short-term variability than either of the midlatitudes.

5.2 Layer Mass

In the average annual period in north midlatitudes (Fig. 5.2a), the absolute maximum in layer mass is seen in late July, with a smaller secondary maximum found in February. The absolute minimum is seen towards the start of May, while a smaller secondary minimum is found in November. Overall the average annual period is relatively smooth, although some short-term variability is present. Most notable in this figure is the high contrast seen between the absolute maximum and minimum values of mass in the isentropic layer. The presence of the semiannual cycle in addition to the annual cycle is something not seen earlier in the average annual period of JAPE in the north midlatitudes.

The south midlatitudes (Fig. 5.2b) have a surprisingly similar pattern to that seen in the north midlatitudes. Maxima are found in February, August, and December, although the primary maximum is that seen in February. Minima are also seen in May and September, although the primary minimum is that seen in May. Also seen is a jagged average annual period with increased short-term variability in comparison to what was seen in the north midlatitudes.

The average annual period for the tropics (Fig. 5.2c) shows a pattern quite different from those seen in the midlatitudes, yet similar to tropical JAPE. Like the south midlatitudes, a maximum in layer mass is seen in early February, while like the north midlatitudes, a minimum is found in November. In addition to these absolute values, relative maxima/minima pairs are seen every one to two months, as previously seen with the average annual period of tropical JAPE. In comparison to the midlatitudes, this jagged average annual period suggests much more short-term variability.

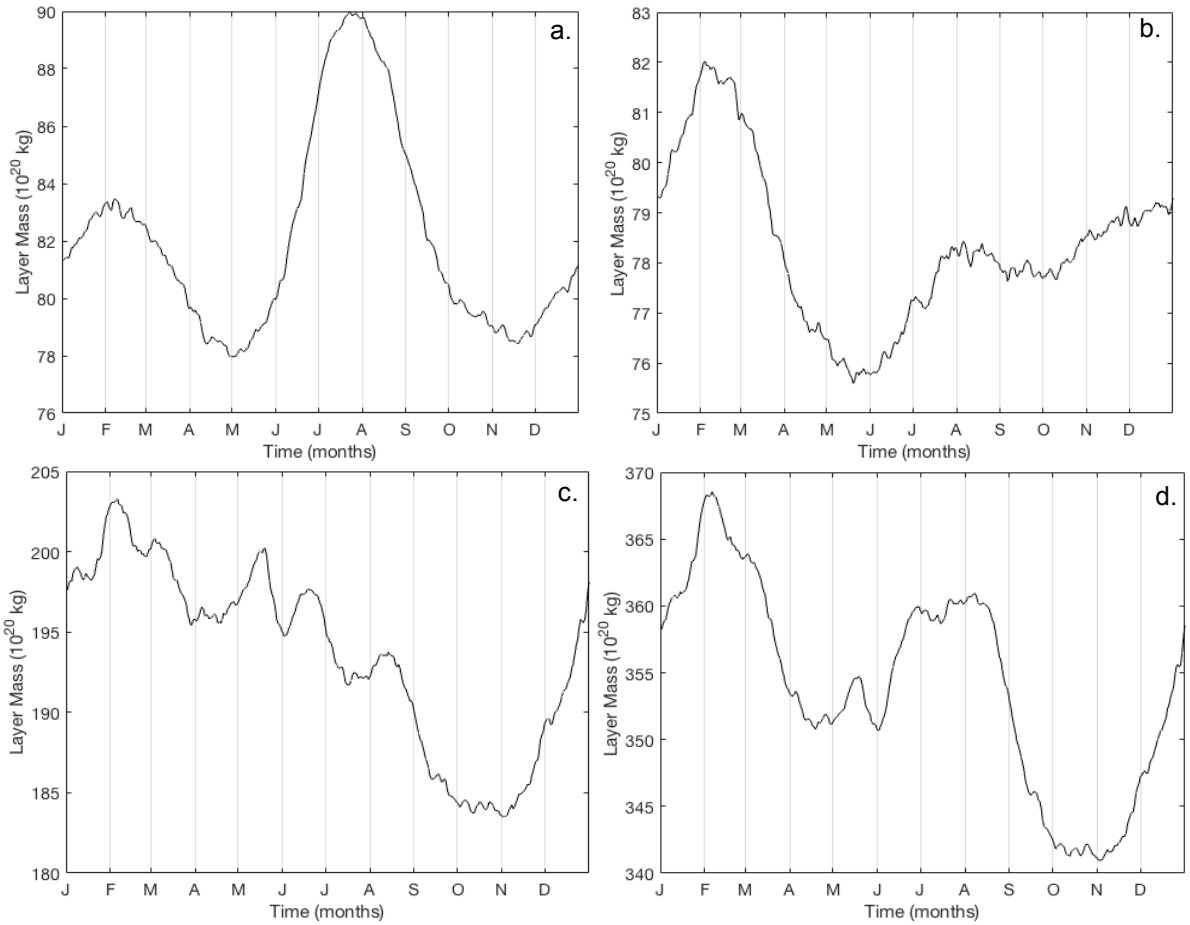

Figure 5.2: Average annual period of isentropic mass at the 356 K-420 K layer, calculated from the entire the 38-year period. (a) North midlatitudes (30˚N-60˚N). (b) South midlatitudes (30˚S-60˚S). (c) Tropics (30˚S-30˚N). (d) Non-polar regions (60˚S-60˚N).

Finally, the average annual period of the nonpolar region (Fig. 5.2d) has an appearance most similar to the combination of the tropics and the south midlatitudes. The maximum of layer mass is found once more in February, while the minimum again falls in November. A secondary maximum plateaus across June, July, and August, with secondary minima in April and June. Although less jagged than the tropics, and arguably the south midlatitudes, the nonpolar region still contains more short-term variability than the north midlatitudes.

6. Analysis of Subannual Variability

As earlier analysis placed emphasis on deciphering the annual cycle of JAPE and layer mass, additional steps for statistical analysis are performed to further investigate variability on a subannual scale by smoothing and removing the harmonics associated with the annual cycle.

After creating the average annual period for each quantity as described in Section 5, the average annual period is tripled, to allow for consideration of the points leading up to the start of each cycle, and those following the end of each cycle. After that, an eleven-point, and then a seventeen-point running mean are applied to this new series, and the middle year of the three is isolated and subtracted from the daily-averaged data of the entire 38-year time series. This results in the departures from the average annual period, seen in Figs. 6.1, depicting JAPE, and 6.2, depicting layer mass.

Most notably, the time series for both tropical and nonpolar JAPE and layer mass look highly similar to their respective unaltered counterparts, especially when comparing Figs. 6.1c and 6.1d to Figs. 3.2a and 3.2b. The time series of JAPE and layer mass in the midlatitudes appears to be much messier, with less of a resemblance to their unaltered counterparts. As seen before in Section 3, Figs. 6.1c and 6.1d look similar to each other, as do Figs. 6.2c and 6.2d. However, the similarities between JAPE and layer mass for these regions are reduced, as the times series of layer mass in the tropics and nonpolar region is also “messier”. The annual cycle has clearly been removed, although seasonal variation is still very much present. This suggests that variability outside of the annual cycle may play a larger role than previously indicated, especially in the tropics.

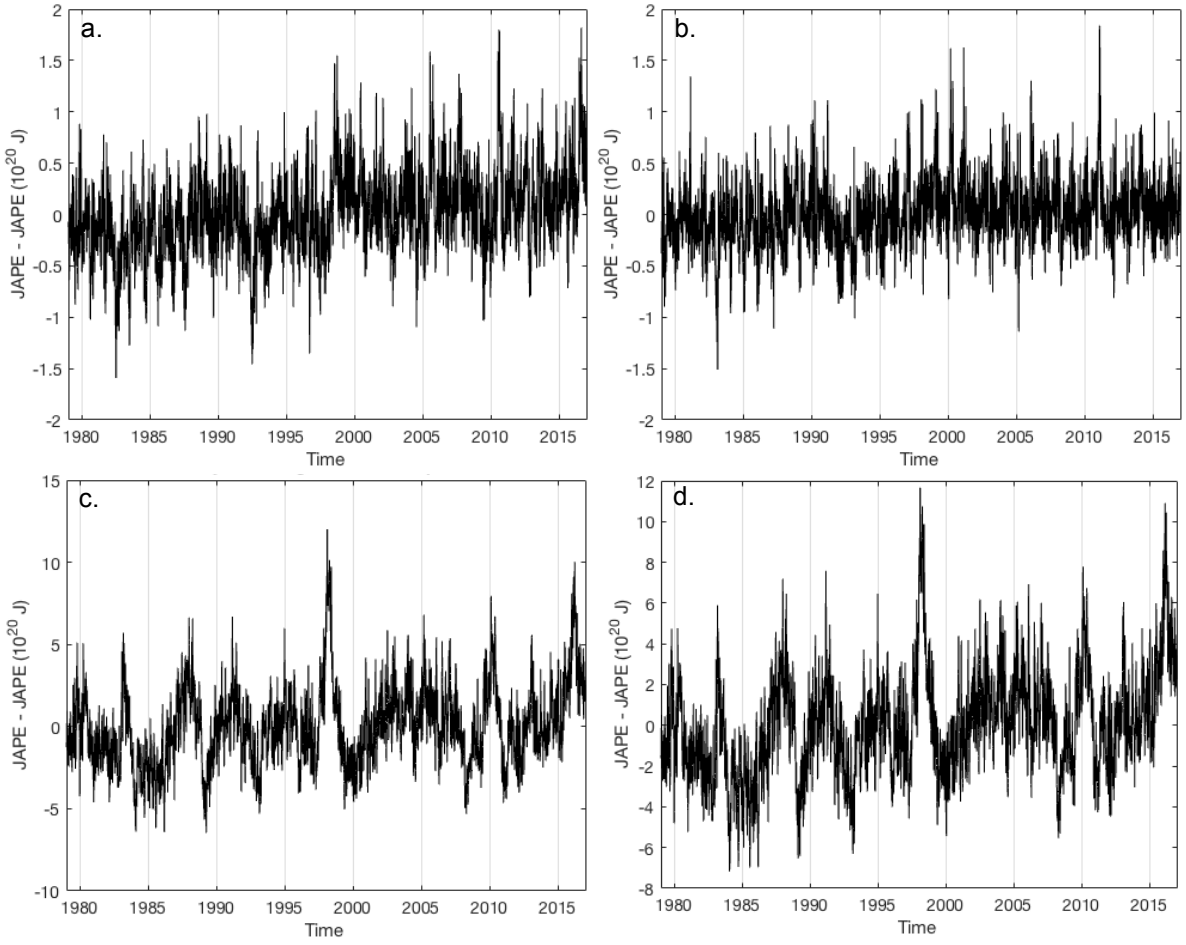

Figure 6.1: Time series of departures from the average annual cycle of isentropic JAPE in the 356 K-420 K layer over the 38-year period from 00Z 01 January 1979 to 18Z 31 December 2016. (a) North midlatitudes (30˚N-60˚N). (b) South midlatitudes (30˚S-60˚S). (c) Tropics (30˚S-30˚N). (d) Non-polar regions (60˚S-60˚N).

In order to gain further insight on the short-term variability, spectral analysis of these new time series is performed once more by computing the PSD through the use of Welch's overlapped segment averaging estimator. For this analysis, a Hamming window function is used again, with 50 percent overlap between windows of two years' length. Statistical significance is computed via chi-squared testing with 99.99% confidence limits, using an AR(1) process computed from the new time series as a null hypothesis. The results from this new spectral analysis can be seen in Figs. 6.3 and 6.4.

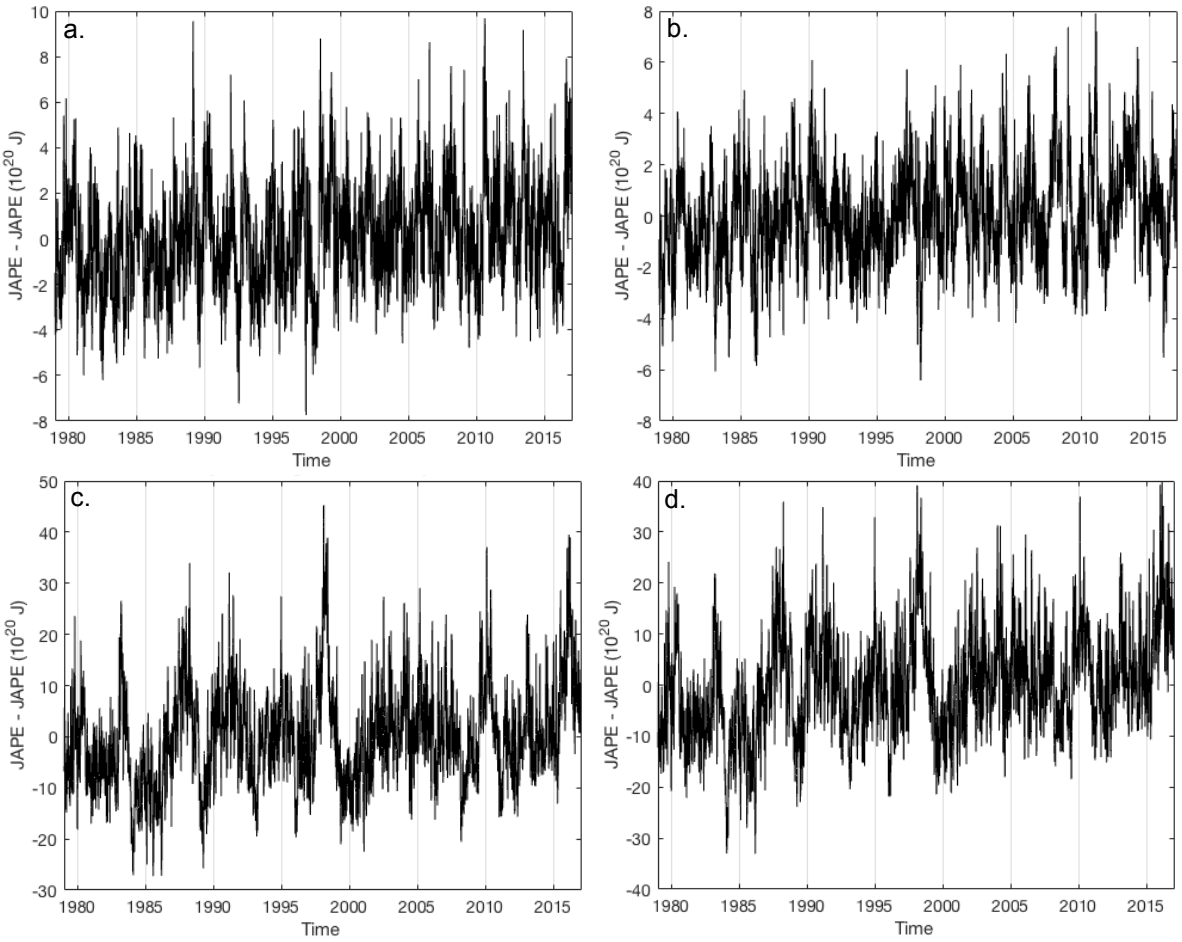

Figure 6.2: Time series of departures from the average annual cycle of isentropic layer mass in the 356 K-420 K layer over the 38-year period from 00Z 01 January 1979 to 18Z 31 December 2016. (a) North midlatitudes (30˚N-60˚N). (b) South midlatitudes (30˚S-60˚S). (c) Tropics (30˚S-30˚N). (d) Non-polar regions (60˚S-60˚N).

In the north midlatitudes (Fig. 6.3a), additional spectral analysis of isentropic JAPE shows that periods between 7.8 and 45.6 days are significant with 99.99% confidence. A similar range of short-term variability is seen in the south midlatitudes (Fig. 6.3b) as well, indicating that periods between 6.9 and 35.8 days are significant. The tropics (Fig. 6.3c) and the nonpolar regions (Fig. 6.3d) are once more nearly identical to each other, with a wider range of short-term variability, confirming that periods ranging from 8.5 to 91.3 days are significant.

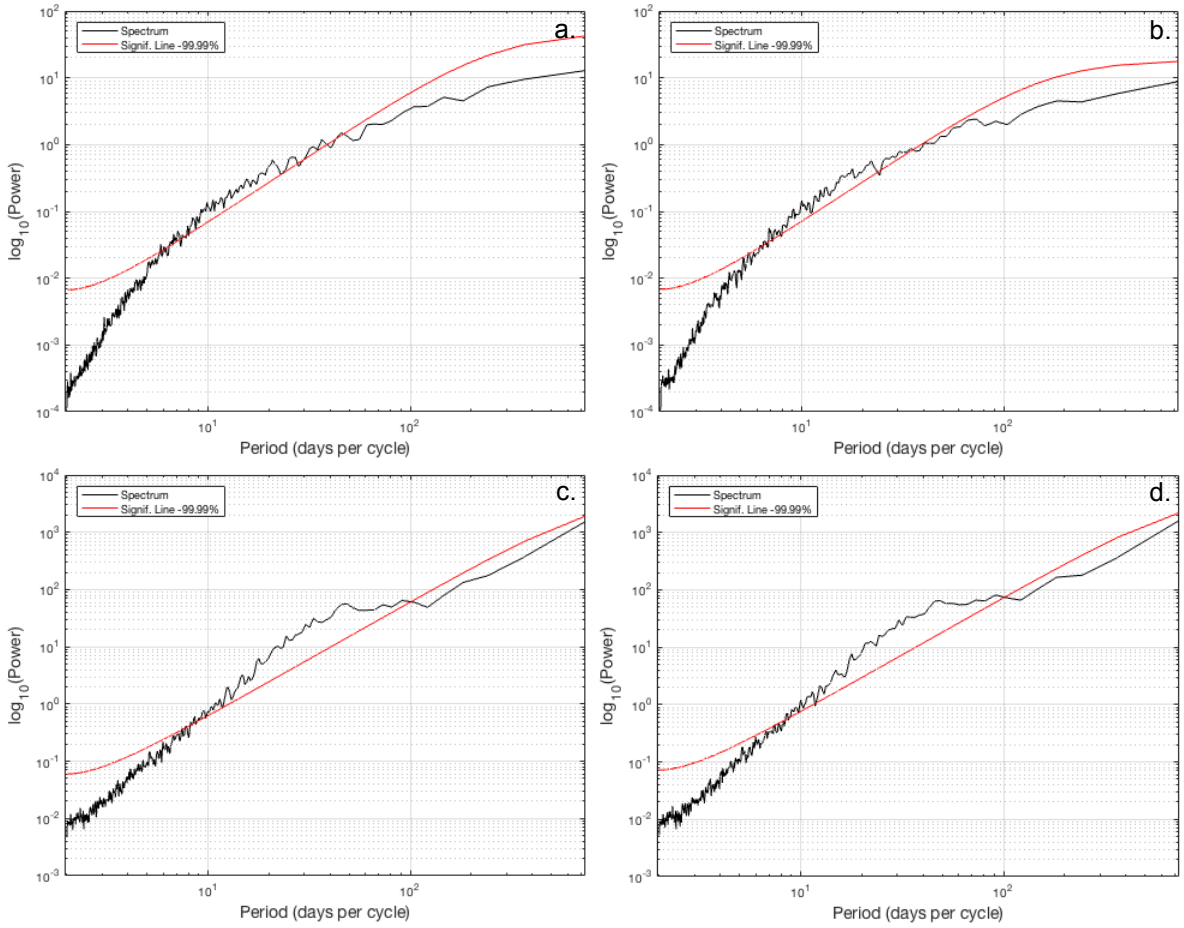

Figure 6.3: Spectral analysis of the departures from the average annual cycle of isentropic JAPE in the 356 K-420 K layer over the 38-year period from 00Z 01 January 1979 to 18Z 31 December 2016. (a) North midlatitudes (30˚N-60˚N). (b) South midlatitudes (30˚S-60˚S). (c) Tropics (30˚S-30˚N). (d) Non-polar regions (60˚S-60˚N).

Similar to JAPE, additional spectral analysis of isentropic layer mass in the north midlatitudes (Fig. 6.4a) shows that periods between 6.6 and 29.2 days are significant with 99.99% confidence. A slightly shorter range of short-term variability is seen in the south midlatitudes (Fig. 6.4b), indicating that periods between 6.1 and 19.2 days are significant. The tropics (Fig. 6.4c) and the nonpolar regions (Fig. 6.4d) are once again effectively identical, with significant periods of mass fluctuation ranging from 9.5 to 91.3 days.

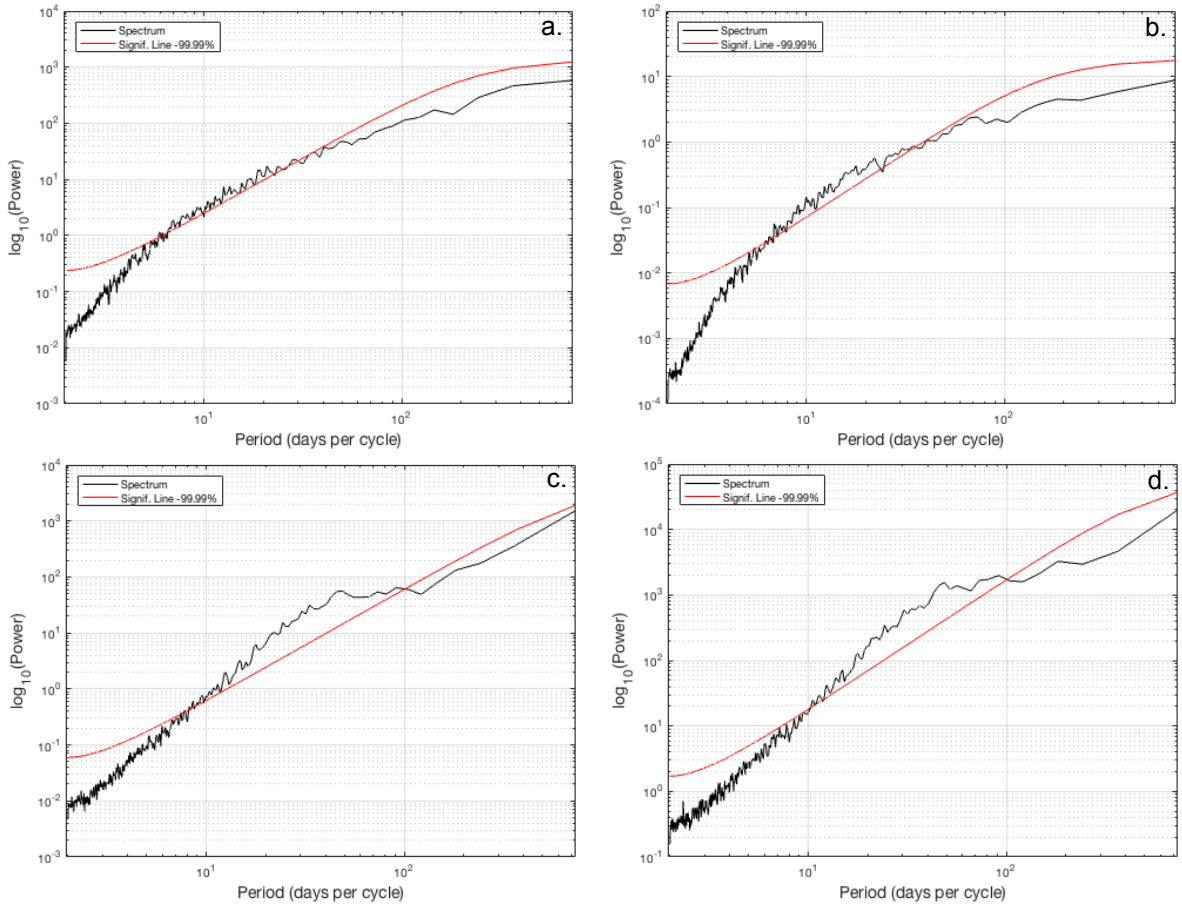

Figure 6.4: Spectral analysis of the departures from the average annual cycle of isentropic layer mass in the 356 K-420 K layer over the 38-year period from 00Z 01 January 1979 to 18Z 31 December 2016. (a) North midlatitudes (30˚N-60˚N). (b) South midlatitudes (30˚S-60˚S). (c) Tropics (30˚S-30˚N). (d) Non-polar regions (60˚S-60˚N).

7. Concluding Discussion and Summary

To summarize what is known so far, circulations brought about by tropical cyclones and convective storms effectively transform the energy that they process into potential energy. Much of this energy then becomes trapped in the UTLS as the JAPE bubble. The energy will accumulate there until it is released through extratropical interactions, which create weaknesses in the inertial walls that hold the bubble in place, leading to poleward surges of JAPE. These tropical plumes conveying energy poleward appear to occur in periodic bursts. As the inertial wall is routinely weakened by extratropical waves, if no waves are generated, energy will continue to accumulate until the wall is weakened by the amount of energy it contains, leading to anomalous, strong surges.

A recent study, similar to what was performed here, sought to produce a time series of significant intraseasonal variability in APE in the northern hemisphere and identify synoptic-scale variability from that data set (Wintels and Gyakum 1999)[1]. The study found a 3-day cycle in APE generation, while the time scale of depletion events remained consistent with that of baroclinic instability observations of developing synoptic eddies.

The focus of this study was to examine the periodic nature of the fluctuation of energy levels found in the JAPE bubble, initially noticed in examination of time series of layer-averaged JAPE. Spectral analysis of the JAPE bubble yielded prevailing peaks in frequency seen at periods equal to 0.5, 1, 121.7, 182.8, and 366.0 days per cycle. Spectral analysis of layer mass in the tropics yielded significant peaks in frequency seen at periods equal to 1, 119.6, 182.8, and 366.0 days per cycle. Additionally, comparison of the average

[1] It is should be noted that the author of this study was made aware of the Wintels and Gyakum (1999) study well after designing this study. With this in mind, similarities between the two must be attributed to coincidence.

annual patterns in the JAPE cycle yielded interesting implications about how each latitudinal region participates in the periodicity of the JAPE bubble, and related layer mass.

7.1 Annual Variability

The most apparent and most frequently significant period found in analysis of isentropic JAPE and layer mass is the annual cycle. First seen through visual inspection of the time series, the annual cycle was confirmed to be significant through spectral analysis, and reaffirmed through analysis of the average annual period. Overall, the annual cycle proves to be dominant over all other cycles seen in all regions analyzed, which is especially apparent in Fig. 5.1.

As predicted, the midlatitudes of each hemisphere experience a maximum value of both JAPE and layer mass during their respective summer months, a result expected due to planetary differential heating and increased convective production of APE. Additionally, mass and energy transport out of the bubble becomes more sporadic, as extratropical interactions induced by the polar jet are effectively nonexistent in the summer hemisphere. This reverses during their respective winter months, with JAPE and layer mass falling off significantly to reach a minimum value. During the winter, energy and mass input to the bubble is decreased, while energy and mass transfer out of the bubble increases, due to the reappearance and maintenance of the polar jet.

One notable difference in the average annual periods of JAPE in the north and south midlatitudes lies in the amplitude of each annual cycle, where the north midlatitudes feature a much larger difference between the maximum and minimum values of JAPE than the south midlatitudes. One hypothesis for why this occurs approaches the difference in magnitudes

from the perspective of energy transfer from the bubble. As stated before, climatologically, the southern hemisphere has a stronger, more persistent polar jet than the northern hemisphere. This could suggest a more regular flow of energy out of the JAPE bubble, via jet connections occurring more frequently in austral winter. As the polar jet in the northern hemisphere occurs on a more sporadic basis, connections with the subtropical jet are sparse. It is possible that the extratropical interactions which free energy from the JAPE bubble occur more prevalently in the southern hemisphere, resulting in the routine weakening of the retaining inertial wall to permit plumes of energy to burst forth towards the poles.

In the tropics, the annual cycle of JAPE takes on an appearance most similar to the annual cycle of the southern hemisphere. The persistent nature of the southern RWT, combined with a long-lived southern polar jet indicates that energy transport through the southern hemisphere may dominate JAPE patterns on the annual scale.

7.2 Semiannual Variability

Inspection of the spectra of JAPE for northern and southern midlatitudes results in a semiannual cycle for JAPE. Interestingly, this is not easily visible when looking at the time series, and certainly not the average annual period for either region. Additionally, although not present in the tropics alone, the semiannual cycle reappears when combining the tropics and midlatitudes to form the nonpolar region. The average annual period of layer mass in the midlatitudes differs from that of JAPE, where the semiannual cycle competes with the annual cycle. Although the amplitudes are set opposite, the north and the south midlatitudes have become more temporally synchronized (Fig. 5.2a-b) Spectral analysis confirms this is present in layer mass in all four latitudinal regions.

Typically, seasonal variation of isentropic zonally averaged mass has been attributed to planetary scale differential heating (Townsend and Johnson 1985). This explanation fits well with the midlatitudes, given that each season will also experience variation in radiational heating as the earth's orbit allows for a changing angle of incidence. However, as the tropics experience less changes overall in heating, this cycle becomes less prevalent. In combining the tropics with the midlatitudes, the semiannual cycle grows in significance once again, likely due to the seasonal cycle that as a result of the superposition of the large, north midlatitudinal maximum over a tropical minimum, as well as coincidence of tropical and south midlatitudinal maxima. The presence of the semiannual cycle in tropical layer mass and its absence in JAPE remains an interesting question that must still be answered.

7.3 Seasonal Variability

In the initial spectral analysis performed in Section 4, seasonal analysis was not found to be statistically significant. However, a small range of frequencies around 50 days per cycle stood out from the spectrum of layer mass and JAPE in the tropics and nonpolar region, seen in Figs. 4.1c-d and 4.2c-d, prompting additional spectral analysis with the annual cycle and its associated harmonics removed. This analysis of subannual variability, performed in Section 6, confirmed significant seasonal-scale periods of mass and energy fluctuations in the tropics and nonpolar regions. More specifically, these periods were found ranging from around 10 to 90 days. One possible cause for this range could be the convection seen to occur on a 30- to 60- day cycle with the MJO acting as a source for APE and inflating the bubble. Conversely, the occurrence of the MJO could force extratropical interactions with the JAPE bubble, thus allowing for the release of energy.

Recent research supports the hypothesis for MJO involvement in the extratropical interactions that free energy from the bubble. One study found strong coherence between the subtropics and the tropics, supporting the suggestion that planetary wave baroclinic instability, and the MJO are interconnected (Straus and Lindzen 1999). Another study found that, in all phases of the MJO, modeling and observational studies revealed that 300 hPa height anomalies formed part of an MJO-like global wave train. (Barrett and Henley 2015). Additional work has indicated that the structure and evolution of midlatitudinal setups are statistically connected to tropical convection on a 30-60 day time scale. (Schubert and Park 1991; Hsu 1996). Overall, although this study does not seem to outright support involvement of the MJO in the temporal variability of the JAPE bubble, the possibility must not yet be rejected.

7.4 Predicted Cycles Not Seen

As mentioned in the introduction, the length of the dataset used in analysis should be sufficient to see signals of long-term temporal variability. No such variability was seen through spectral analysis, and was not easily identifiable through time series analysis.

Interestingly, large peaks in both JAPE and layer mass in the tropics and nonpolar region were visible in Figs. 3.2a-b and 3.5c-d on a 4-7 year period. Most notably, these peaks occur in 1983, 1998, 2010, and 2016, among others, coinciding with years of heavy El Niño activity (Physical Sciences Division 2016). Although this paper has not made an effort to quantify any correlation, initial analysis indicates this is a path that requires additional exploration to further understanding.

7.5 Future Work

As this serves primarily as a climatological survey of JAPE fluctuations, there is still much to be studied within this topic. One major area requiring further attention is the analysis of the JAPE budget, particularly in quantifying energy import and export values and processes. This is of particular importance when considering the nonpolar region as a whole, which encompasses the core of the JAPE bubble, as well as the plumes that siphon energy to the poles. This could be accomplished in part through cross-spectral analysis, which would help in understanding how the tropics and mid-latitudes interact with each other.

Additional future research will entail analysis of extreme meteorological events, relating high-impact observations to high and low values found within single-year time series to learn more about the physical processes that affect the build-up and release of JAPE. Related research analyzing jet superposition events has been conducted extensively by Winters and Martin (2014; 2016; 2017), and shows that the vertical superposition of the STJ and polar jet often results in extreme weather. Initial observational analysis indicates that the transfer of energy via jet connections often coincides geographically and temporally with extreme weather events. This would imply that monitoring the JAPE bubble and the relative positions of the jets could be of use in forecasting for large-scale severe weather.

Finally, expansion of the current dataset could provide insight regarding JAPE variability with respect to global climate change. The overall warming of the poles weakens the temperature gradient between the poles and the midlatitudes. This leads to irregular formation of the polar jet, corresponding with less frequent controlled transfers of energy. Although a threshold, or a critical mass of the JAPE bubble has not yet been encountered, arrival at such a critical point would potentially lead to more common violent poleward

explosions. As indicated earlier, large releases of energy from the bubble often fuel extreme weather outbreaks at the surface. This would suggest a new method for investigating the idea of increased severe weather caused by global climate change.

REFERENCES

American Meteorological Society, 2012: "available potential energy." Glossary of Meteorology. [Available online at http://glossary.ametsoc.org/wiki/Available_potential_energy].

Anthes, R. A. and D. R. Johnson, 1968: Generation of available potential energy in Hurricane Hilda (1964). *Mon. Wea. Rev.*, **113**, 323-338.

Barrett, B. S., and B. N. Henley, 2015: Intraseasonal Variability of Hail in the Contiguous United States: Relationship to the Madden–Julian Oscillation. *Mon. Weather Rev.*, **143**, 1086–1103.

Chimonas, G., and R. Rossi, 1987: The Relationship between Tropopause Potential Temperature and Buoyant Energy of Storm Air. *J. Atmos. Sci.*, **44**, 2902–2910.

Dee, D. P., and Coauthors, 2011: The ERA-Interim reanalysis: configuration and performance of the data assimilation system. *Quart. J. Roy. Meteor. Soc.*, **137**, 553–597.

Dopplick, T. G., 1972: Radiative Heating of the Global Atmosphere. *J. Atmos. Sci.*, **29**, 1278–1294.

Dutton, J. A., and Johnson, D. R., 1967: The theory of available potential energy and a variational approach to atmospheric energetics. *Adv. Geophys.*, **12**, 333-436.

Folkins, I., S. J. Oltmans, and A. M. Thompson, 2000: Tropical convective outflow and near surface equivalent potential temperatures. *Geophys. Res. Lett.*, **27**, 2549-2552.

Gettelman, A., and P. M. de F. Forster, 2002: A Climatology of the Tropical Tropopause Layer. *J. Meteor. Soc. Japan*, **80**, 911–924.

——, P. M. de F. Forster, M. Fujiwara, Q. Fu, H. Vömel, L. K. Gohar, C. Johanson, and M. Ammerman, 2004: Radiation balance of the tropical tropopause layer. *J. Geophys. Res.*, **109**, D07103.

Hartmann, D. L., 2005: ATM S 552 Course Notes. 12–13, 127–137. [Available online at http://www.atmos.washington.edu/~dennis/552_Notes_ftp.html].

Hsu, H. H., 1996: Global view of the intraseasonal oscillation during northern winter. *J. Clim.*, **9**, 2386–2406.

Holton, J. R., 2004: *An Introduction to Dynamic Meteorology*. Fourth Ed. Elsevier Academic Press.

Johnson, D. R., 1989: The forcing and maintenance of global monsoonal circulations: An isentropic analysis. *Adv. Geophys.*, **31**, 43–329.

Kalnay et al., 1996: The NCEP/NCAR 40-year reanalysis project. *Bull. Amer. Meteor. Soc.*, **77**, 437-470.

Krishnamurti, T. N., 1961a: The Subtropical Jet Stream of Winter. *J. Meteor.*, **18**, 172–191.

——, 1961b: On the Role of the Subtropical Jet Stream of Winter in the General Circulation. *J. Meteor.*, **15**, 657–670.

Lorenz, E. N., 1955: Available Potential Energy and the Maintenance of the General Circulation. *Tellus A*, **7**, 157–167.

Margules, M., 1903: Über die energie der sturme. *Jahrb. Zentralanst. Meteor.*, 1–26 (Translation by C. Abbe (1910) in *Smithsonian Institute Miscellaneous Collection* **51**, 553-595).

MathWorks, ed., 2017: Signal Processing Toolbox Reference. The MathWorks, Inc., Natick, MA, 1642–1663 [Available online at https://www.mathworks.com/help/pdf_doc/signal/signal_ref.pdf].

Mecikalski, J. R. and G. J. Tripoli, 1998: Inertial Available Kinetic Energy and the Dynamics of Tropical Plume Formation. *Mon. Wea. Rev.*, **126**, 2200-2216.

Mecikalski, J. R. and G. J. Tripoli, 2003: Influence of upper-tropospheric inertial stability on the convective transport of momentum. *Quart. J. Roy. Meteor. Soc.*, **129**, 1537-1563.

Palmén, E., 1951: The rŏle of atmospheric disturbances in the general circulation. *Quart. J. Roy. Meteor. Soc.,* **77**, 337–354.

Pauluis, O., 2007: Sources and Sinks of Available Potential Energy in a Moist Atmosphere. *J. Atmos. Sci.*, **64**, 2627–2641.

Physical Sciences Division, 2016: Past ENSO events used in dashboard: Top 7 El Nino events for 148-2015. National Oceanic and Atmospheric Administration, Earth System Research Laboratory, Boulder, CO. [Available online at https://www.esrl.noaa.gov/psd/enso/events.html].

Schubert, S. D., and C. K. Park, 1991: Low-Frequency Intraseasonal Tropical-Extratropical Interactions. *J. Atmos. Sci.*, **48**, 629–650.

Shapiro, M. A., T. Hampel, and A. J. Krueger, 1987: The Arctic Tropopause Fold. *Mon. Wea. Rev.*, **115**, 444–454.

Straus, D. M., and R. S. Lindzen, 2000: Planetary-Scale Baroclinic Instability and the MJO. *J. Atmos. Sci.*, **57**, 3609–3626.

Townsend, R. D., and D. R. Johnson, 1985: A Diagnostic Study of the Isentropic Zonally Averaged Mass Circulation during the First GARP Global Experiment. *J. Atmos. Sci.*, **42**, 1565–1579.

Tripoli, G. J., and E. A. Smith, 2014a: Introducing Variable-Step Topography (VST) coordinates within dynamically constrained Nonhydrostatic Modeling Systems (NMW), part 1: VST formulation within NMS host model framework. *Dyn. Atmos. Ocean.*, **66**, 28–57.

——, and ——, 2014b: Introducing Variable-Step Topography (VST) coordinates within dynamically constrained Nonhydrostatic Modeling Systems (NMW), part 2: VST performance on orthodox obstacle flows. *Dyn. Atmos. Ocean.*, **66**, 10–27.

Tripoli, G. J., and L. E. Nytes, 2017: On JAPE. *TBD*,.

Wintels, W., and J. R. Gyakum, 2000: Synoptic climatology of Northern Hemisphere available potential energy collapses. *Tellus, Ser. A Dyn. Meteor. Oceanogr.*, **52**, 347–364.

Winters, A. C., and J. E. Martin, 2014: The role of a polar/subtropical jet superposition in the May 2010 Nashville Flood. *Wea. Forecasting*, **29**, 954-974.

Winters, A. C., and J. E. Martin, 2016: Synoptic and mesoscale processes supporting vertical superposition of the polar and subtropical jets in two contrasting cases. *Quart. J. Roy. Meteor. Soc.*,**142**, 1133-1149.

Winters, A. C., and J. E. Martin, 2017: Diagnosis of a North American polar/subtropical jet superposition employing potential vorticity inversion. *Mon. Wea. Rev.*,**145**, 1853-1873.